This is an open access article published under a Creative Commons Attribution (CC-BY) License, which permits unrestricted use, distribution and reproduction in any medium, provided the author and source are cited.

ACS AUTHORCHOICE

energy&fuels

pubs.acs.org/EF

Article

Combustion of n-C_3−C_6 Linear Alcohols: An Experimental and Kinetic Modeling Study. Part I: Reaction Classes, Rate Rules, Model Lumping, and Validation

M. Pelucchi,* S. Namysl, E. Ranzi, A. Rodriguez, C. Rizzo, K. P. Somers, Y. Zhang, O. Herbinet, H. J. Curran, F. Battin-Leclerc, and T. Faravelli

Cite This: *Energy Fuels* 2020, 34, 14688−14707

Read Online

ACCESS | Metrics & More | Article Recommendations | Supporting Information

ABSTRACT: This work (and the companion paper, Part II) presents new experimental data for the combustion of n-C_3−C_6 alcohols (n-propanol, n-butanol, n-pentanol, n-hexanol) and a lumped kinetic model to describe their pyrolysis and oxidation. The kinetic subsets for alcohol pyrolysis and oxidation from the CRECK kinetic model have been systematically updated to describe the pyrolysis and high- and low-temperature oxidation of this series of fuels. Using the reaction class approach, the reference kinetic parameters have been determined based on experimental, theoretical, and kinetic modeling studies previously reported in the literature, providing a consistent set of rate rules that allow easy extension and good predictive capability. The modeling approach is based on the assumption of an alkane-like and alcohol-specific moiety for the alcohol fuel molecules. A thorough review and discussion of the information available in the literature supports the selection of the kinetic parameters that are then applied to the n-C_3−C_6 alcohol series and extended for further proof to describe n-octanol oxidation. Because of space limitations, the large amount of information, and the comprehensive character of this study, the manuscript has been divided into two parts. Part I describes the kinetic model as well as the lumping techniques and provides a synoptic synthesis of its wide range validation made possible also by newly obtained experimental data. These include speciation measurements performed in a jet-stirred reactor ($p = 10^7$ kPa, $T = 550$−1100 K, $\varphi = 0.5, 1.0, 2.0$) for n-butanol, n-pentanol, and n-hexanol and ignition delay times of ethanol, n-propanol, n-butanol, n-pentanol/air mixtures measured in a rapid compression machine at $\varphi = 1.0$, $p = 10$ and 30 bar, and $T = 704$−935 K. These data are presented and discussed in detail in Part II, together with detailed comparisons with model predictions and a deep kinetic discussion. This work provides new experimental targets that are useful for kinetic model development and validation (Part II), as well as an extensively validated kinetic model (Part I), which also contains subsets of other reference components for real fuels, thus allowing the assessment of combustion properties of new sustainable fuels and fuel mixtures.

1. INTRODUCTION

Alcohols are promising alternative fuels, from the perspective of carbon footprint reduction in the transport sector, as well as being blending fuel components for internal combustion engines. Alcohol-based fuels have the potential to be used in a near CO_2-neutral way, through efficient conversion of lignocellulosic biomass.[1,2] In spark ignition engines, the resistance to ignition, or the antiknocking propensity, of a fuel is characterized by its octane rating, which can be measured as the research octane number (RON) and/or the motor octane number (MON). As suggested by Kalghatgi et al.,[3,4] a better characterization can be obtained by combining the RON and MON to obtain the octane index (OI):

$$\mathrm{OI} = \mathrm{RON} - KS$$

where S is the octane sensitivity ($S = \mathrm{RON} - \mathrm{MON}$) and K is an empirical parameter that is dependent on the pressure and temperature conditions of the engine. Commercial gasoline fuel RON and MON values are typically in the range of 90−100 and 82−90, respectively. The counterpart to the octane rating in compression ignition engines is the cetane number (CN), which, instead, represents the propensity for a fuel to ignite, with commercial diesel fuels having CNs in the range of 45−55.

Figure 1 compares the RON, MON, and CN values for methanol, ethanol, and linear n-C_3−C_8 alcohols (represented by bars in Figure 1) with those of commercial gasoline and diesel fuels (shaded areas in Figure 1), as reported by Sarathy et al.[5] and by the U.S. National Renewable Energy Laboratory (NREL).[6] Methanol, ethanol, propanol, and butanol have octane ratings comparable or higher than that of commercial gasoline fuels. In addition, their octane sensitivity ($S = \mathrm{RON} - \mathrm{MON}$), matches or exceeds that of commercial gasoline fuels ($S \approx 10$), making them suitable for modern low-temperature combustion (LTC) and direct-injection spark-ignition engines.[7] Higher-molecular-weight alcohols ($\geq C_5$) have lower knock resistance (i.e., a lower octane rating), thus preventing their blending with gasoline fuels. However, as the linear carbon chain length increases, the cetane number also increases, approaching

Received: July 7, 2020
Revised: October 2, 2020
Published: October 27, 2020

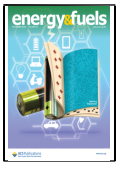

Downloaded via POLITECNICO DI MILANO on June 15, 2022 at 12:55:02 (UTC).
See https://pubs.acs.org/sharingguidelines for options on how to legitimately share published articles.

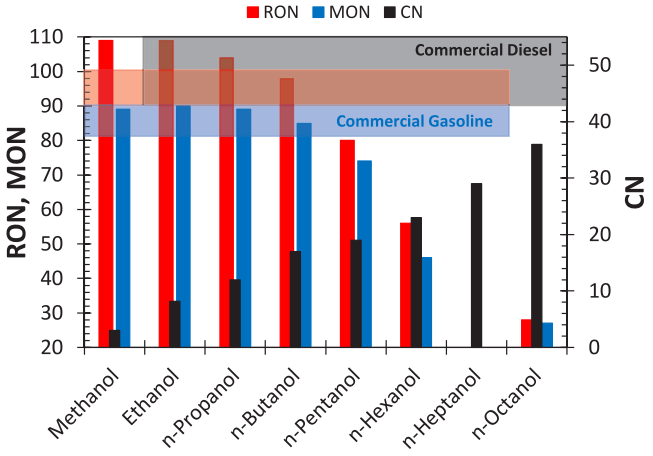

Figure 1. RON (red), MON (blue), and CN (black) values for methanol, ethanol, and linear C_3−C_8 *n*-alcohols (bars) with that of commercial gasoline and diesel fuels (shaded areas).[5,6] Red-shaded and blue-shaded areas correspond to the respective RON and MON ranges for commercial gasoline fuels. Black-shaded area represents the CN range for commercial diesel fuels.

that of commercial diesels, making fuels like *n*-octanol highly suitable for use in compression ignition engines[8] or as blending components in jet engines. Even *n*-pentanol and *n*-hexanol have been successfully tested in diesel engines, both as neat fuels and in blends with commercial diesel or biodiesel fuels.[9−16] In relation to new engine technologies, a recent modeling study investigated the operability maps of *n*-butanol and *n*-pentanol in HCCI engines using a detailed kinetic model.[17] It was found that these fuels largely extend the operability maps toward lower engine loads and higher exhaust gas recirculation, compared to primary reference fuel (PRF) and toluene primary reference fuel (TPRF) mixtures (RON/MON = 80−100).

The development of detailed and predictive combustion kinetic models provides a very efficient tool for the synergistic design of fuels and engines,[18] allowing parametric analyses to explore, interpolate, and extrapolate the propensity for (or the resistance to) ignition of different fuels and fuel blends.[19] Generally, the reactivity of oxygenated biofuels (e.g., alcohols, aldehydes, organic acids) is largely influenced by the presence of an oxygenated functional group that modifies bond dissociation energies and enhances, inhibits, and triggers different reaction pathways compared to the parent fuel molecule (e.g., alkane).[20] The recent interest in biofuels and bio-oils from the fast pyrolysis of biomass has motivated systematic experimental and modeling investigations of different chemical families such as aldehydes,[21−25] acids,[26] and oxygenated aromatics[27−29] to unravel the effects of different oxygenated functional groups on fuel kinetics. Beyond their application as surrogate fuel components,[30] such species are also important intermediates in the oxidation of alternative or conventional hydrocarbon fuels, because they are implicit in the hierarchical nature of complex combustion kinetic models. These previous studies aimed to systematically assess the influence of the oxygenated moieties and to provide a set of consistent rate constants capable of describing the different chemical pathways triggered by the different functions. The present work complements previous studies,[21,26] extending them to linear *n*-C_3−C_6 alcohols. As reviewed recently by Sarathy et al.,[5] a great number of experimental and kinetic modeling studies on alcohols have been reported in the literature. In particular, many efforts have been devoted to the investigation of methanol, ethanol, and the isomers of propanol, butanol, and pentanol. Despite their importance, a more limited number of studies are available for longer-chain alcohols such as *n*-hexanol and *n*-octanol.

Based on available theoretical[31−43] and experimental[44−49] rate constant determinations, as well as on previous comprehensive modeling studies,[5,50−55] this work provides a consistent set of rate constants to describe the pyrolysis and high-temperature combustion and LTC mechanisms of *n*-C_3−C_6 alcohols with specific attention paid to the impact of the hydroxyl functional group. The kinetic model thus obtained is validated by comparison with both the new ignition delay time and speciation measurements presented here and with other targets available in the literature. As a further proof of the validity of the approach and of the rate rules adopted, the model is successfully extended to describe *n*-octanol oxidation (see Part II of this study[56]).

The manuscript is organized as follows. Section 2 presents the rate constants for the different reaction classes needed to describe the pyrolysis and oxidation of alcohols. The lumping approach to describe the LTC chemistry is discussed in Section 3. A synopsis of model validations and performances is presented in Section 4. For a more-detailed discussion on model validations and performances, the reader is referred to Part II of this study.[56]

2. KINETIC MODEL DEVELOPMENT

Models for the combustion of *n*-C_3−C_6 alcohols were proposed in the literature,[50−55,57−61] with *n*-butanol being the most targeted fuel. After the detailed review by Sarathy et al.,[5] Li et al.[54] proposed a kinetic model for the pyrolysis and high-temperature combustion of *n*-propanol and *iso*-propanol. A similar study on *n*-pentanol has been recently presented by Wang et al.[55] Nativel et al.[53] recently measured laminar flame speed for *n*- and *iso*-pentanol, presenting a kinetic model for their high-temperature oxidation. In the context of the CRECK kinetic model, Frassoldati et al.[51] and Grana et al.[52] investigated the high-temperature oxidation of propanol and the butanol isomers, respectively. The model was later extended to the pentanol isomers.[53] A lumped low-temperature mechanism to describe *n*-butanol oxidation was proposed by Pelucchi et al.[20] and was extended, by analogy, to *n*-pentanol to investigate the operability maps of a HCCI engine fueled with *n*-butanol and *n*-pentanol.[17]

Motivated by the new measurements presented and discussed in Part II of this study[56] and by new experimental information presented in the literature since the last developments of the alcohols subset, this work presents an updated single comprehensive kinetic model for *n*-C_3−C_6 alcohols pyrolysis and combustion. Different from the previous comprehensive model by Sarathy et al.,[5] the lumping procedure applied to the low-temperature oxidation and to the fuel radicals for higher-molecular-weight alcohols ($C \geq 5$) allows the generation of a more compact kinetic model. In addition, to the authors' knowledge, the attached kinetic model presents the first attempt to describe the oxidation of *n*-propanol under conditions different from pyrolysis or high-temperature oxidation ($T >$ 1000 K), despite the persistent scarcity of experimental data at lower temperatures.

2.1. Overview of the Model Development. Because of the interest in alcohols as blending components for commercial fuels, the CRECK model attached herein accounts for the combustion chemistry of a variety of species relevant to

https://dx.doi.org/10.1021/acs.energyfuels.0c02251
Energy Fuels 2020, 34, 14688−14707

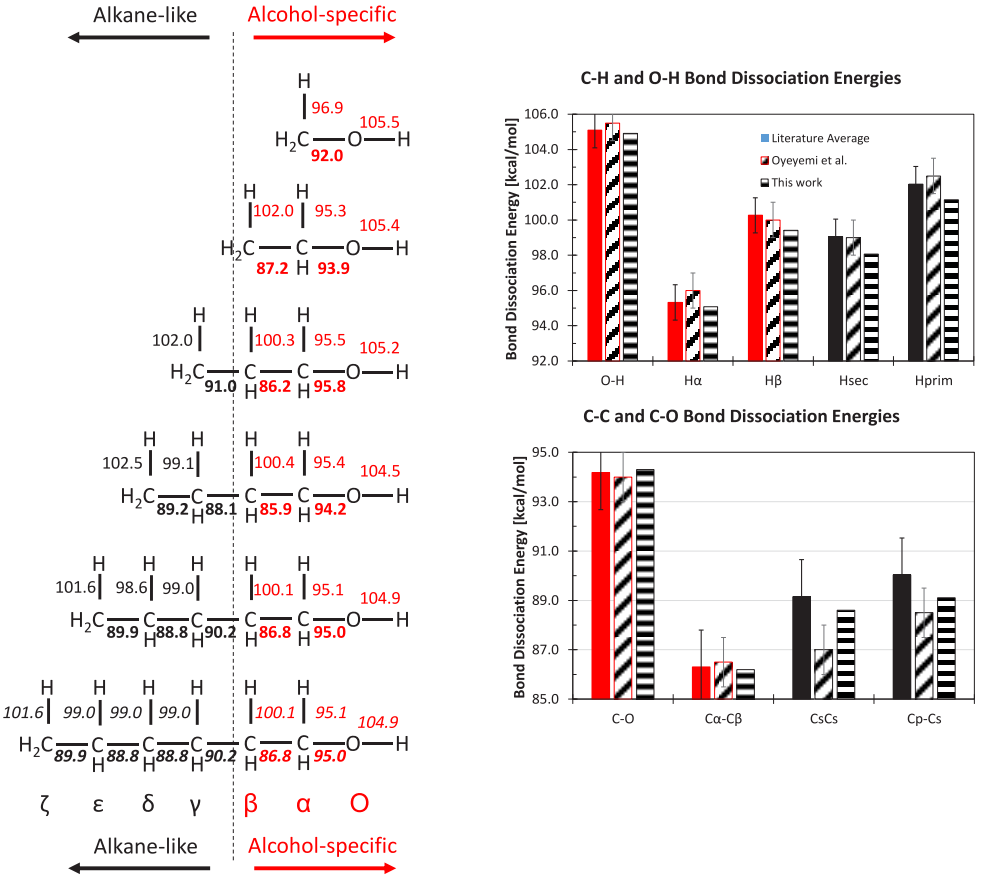

Figure 2. (Left) Bond dissociation energies (BDEs) for C−H bonds,[5] and for C−C bonds (bold).[50,57,69,70,75] BDEs for *n*-hexanol are derived from *n*-pentanol. (Right) Bar diagrams compare BDEs by Oyeyemi et al.[76,77] (diagonal filling) and from previous kinetic studies (full bars), averaged on the *n*-C_3−C_5 alcohol series, with the values calculated from the thermochemical parameters of the kinetic model attached to this study (horizontal filling).

transportation fuels (gasoline, diesel, jet fuels, oxygenated fuels), as documented in detail in the periodically updated webpage.[62] The model can be also used to characterize the formation of pollutants such as polycyclic aromatic hydrocarbons leading to soot formation[63] and NOx.[64] At the core of the kinetic models is the AramcoMech1.3 C_0−C_2 mechanism from Metcalfe and co-workers[65,66] and the C_3 subset from Burke et al.,[67] including the methanol and ethanol subsets. Minor updates from ref 68 have been incorporated in the C_0−C_1 chemistry. The comprehensive kinetic mechanism for high- and low-temperature oxidation consists of 491 species and 17 888 reactions; a description of this mechanism, together with the species nomenclature, is given in the Supporting Information. Of these, 37 species are used to describe the primary oxidation pathways of *n*-C_3−C_6 alcohols. Taking advantage of the modular structure of the CRECK kinetic model, five versions of different size are described in Table S1 in the Supporting Information. These versions are obtained by including or excluding the kinetic subsets to describe the low-temperature chemistry, as well as NOx[64] and PAHs formation.[63] The thermodynamic properties have been adopted from ATcT tables[69,70] (as described in the work of Bagheri et al.[68]) or from the work of Metcalfe et al.[65] and Burke et al.[67] Thermodynamic properties for *n*-C_3−C_6 alcohols are derived from group additivity[71] with updated values from Burke et al.[67] Transport properties for alcohols and derived radicals are from previous kinetic studies.[51−53,61]

As previously discussed in the literature,[50,52,53,57−59,72] it is convenient to treat the oxidation of higher-molecular-weight alcohols by coupling the specific features (i.e., reaction classes, rate rules, alternative pathways) of an alcohol moiety, influenced by the presence of the hydroxyl group (R−OH), and an alkane-like function. The same approach has been recently generalized for different oxygenated fuels[20] and has been applied to the systematic investigation of *n*-C_4−C_6 aldehydes[21] and *n*-C_4−C_5 organic acids.[26] In this work, the collection of theoretical and experimental information from the literature and a thorough assessment of different experimental targets permits the formulation of rules of general validity for the alcohol-specific moiety. The alkane-like moiety is treated according to rate rules already validated for *n*-alkanes,[73,74] also considering possible interactions with the alcohol-specific moiety (e.g., through isomerization reactions). Figure 2 supports the above assumptions showing bond dissociation energies (BDEs) at T = 298 K for different alcohol molecules, as reported in previous combustion kinetic studies.[5,50,57,75] BDEs for methanol and ethanol are from the ATcT Tables.[69,70] BDEs for *n*-hexanol are extrapolated from *n*-pentanol.

The different theoretical methods adopted for BDEs calculations (e.g., CBS-QB3, G4) in previous studies have comparable degrees of uncertainty (±1.5−2.0 kcal mol^{-1}). More accurate calculations (i.e., ± 1.0 kcal mol^{-1}) have been reported in the systematic studies on oxygenated molecules by Oyeyemi et al.[76,77] Bar diagrams in Figure 2 compare BDEs by Oyeyemi et al. and from previous kinetic studies, averaged on the *n*-C_3−C_5 alcohol series, with the values calculated from the thermochemical parameters of the kinetic model attached to this study. A generally good agreement is observed for C−H, O−H,

https://dx.doi.org/10.1021/acs.energyfuels.0c02251
Energy Fuels 2020, 34, 14688−14707

C−C, and C−O BDEs (<2 kcal mol^{-1}). Maximum differences of ≤1 kcal mol^{-1} are observed for C−H and O−H BDEs.

Starting from the alcohol-specific moiety, the hydroxyl function (O−H) has the strongest bond in alcohol fuel molecules. BDEs are in the range of 104−106 kcal mol^{-1}, with an average value of ∼105 kcal mol^{-1}. The electron-withdrawing hydroxyl moiety strongly reduces the BDE of the secondary C−H bond in the α-position (∼95 kcal mol^{-1}), compared to typical values of secondary C−H bonds in alkanes (BDE ≈ 98.5 kcal mol^{-1}). The presence of the hydroxyl function also influences the strength of the secondary C−H bond in the β-position, where the average value of ∼100 kcal mol^{-1} is 1−2 kcal mol^{-1} higher than that of a secondary C−H in corresponding alkanes. From the γ-position onward, it is widely assumed that the influence of the oxygenated function disappears.[20] BDEs for secondary (∼98.5 kcal mol^{-1}) and primary (∼101.5 kcal mol^{-1}) C−H bonds are consistent with those of alkane molecules (98.4 and 101.4 kcal mol^{-1}).[69,70] The C−O bond connecting the hydroxyl function to the carbon chain shows a BDE of ∼94 kcal mol^{-1}. The weakest C−C bond is that connecting the secondary carbons at the α- and β-positions for *n*-propanol, *n*-butanol, *n*-pentanol, and *n*-hexanol. Its BDE of ∼86 kcal mol^{-1} is ∼1−1.5 kcal mol^{-1} lower than that of secondary carbons in alkanes (BDE = 87.5 kcal mol^{-1}).[69,70]

Larger differences with the calculations of Oyeyemi[76,77] are observed for secondary C−C bonds of the alkane-like moieties. Indeed, the average value of 89 kcal mol^{-1} from kinetic studies exceeds that by Oyeyemi by ∼2 kcal mol^{-1}. However, the selected value (i.e., 89 kcal/mol) is consistent with that proposed in the theoretical investigation of *n*-pentanol decomposition by Zhao et al.[78] The same observations can be made for the terminal C−C bond, where a discrepancy of 1.5 kcal mol^{-1} is highlighted. ATcT estimates for *n*-propanol recommend a value of 87.3 kcal mol^{-1} for the terminal C−C bond, in agreement with the estimate from Pelucchi et al.[20] ATcT values span the range of 87.5−89 kcal mol^{-1} (from refs 69 and 70) in the parent alkane molecules moving from propane to pentane. Oyeyemi reported a value of 88.5 kcal mol^{-1}, while the average from kinetic studies is ∼90 kcal mol^{-1}, again in agreement with the investigation by Zhao et al.[78] For the purposes of this study and considering the uncertainties in previous BDE assessments, there exist clear indications of a negligible influence of the hydroxyl function beyond the β-position.

Considering the above assumptions, the description of the kinetic rate constants will mostly focus on reaction pathways that are particular to alcohol oxidation, or those that largely differ from similar pathways in the parent alkanes. Aiming at the derivation of rate rules of general validity for *n*-C_3−C_6 alcohols, *n*-butanol is taken as the model molecule for most of the discussion in the following sections. By analogy with reaction classes typically considered to describe the pyrolysis and oxidation of *n*-alkanes,[79−81] Sarathy et al.[5] reported an ensemble of 31 reaction classes to describe alcohol oxidation at high and low temperatures. Referring only to primary reactions of alcohols and to the successive reactivity of fuel radicals having the same carbon skeleton, it is possible to condense the 31 reaction classes of Sarathy et al.[5] into 20 classes, as reported in Table 1.

Contrary to Sarathy et al.,[5] we neglect the discussion on successive decomposition or oxidation pathways of intermediate species such as unsaturated alcohols (enols), aldehydes, and epoxy alcohols. The kinetic subsets for enols are adopted from

Table 1. Reaction Classes for Alcohols Pyrolysis and Oxidation[a]

reaction class	description
1	unimolecular decompositions
2	four-centered molecular decompositions
3	H atom abstractions
4	radical decomposition reactions
5	radical isomerization reactions
6	reactions of O_2 with alcohols radicals to form HO_2 and a C_n aldehyde/enol
7	addition reactions of alcohol radicals to O_2($\dot{R} + O_2 = R\dot{O}_2$)
8	recombination/disproportionation $\dot{R}' + R\dot{O}_2 = R\dot{O} + R\dot{O}$ ($\dot{R}' = \dot{H}$, $\dot{C}H_3$, alcohol radicals)
9	recombination/disproportionation $R'\dot{O}_2 + R\dot{O}_2 = R\dot{O} + R\dot{O}$ ($\dot{R} = \dot{H}$, $\dot{C}H_3$, alcohol radicals)
10	$R\dot{O}_2$ concerted eliminations to form $H\dot{O}_2$ + aldehyde/enol
11	$R\dot{O}_2$ isomerization reactions (RO_2=$\dot{Q}OOH$), including Waddington-type reactions (RO_2 = OH + CH_2O + C_{n-1} aldehyde)
12	$\dot{Q}OOH$ decomposition to form $\dot{O}H$ + alkenes/enols + carbonyl compounds
13	$\dot{Q}OOH$ decomposition to form $H\dot{O}_2$ + $C_n$enols
14	$\dot{Q}OOH$ cyclization to form $\dot{O}H$ and epoxy (heterocyclic) alcohols
15	dehydration of $\dot{Q}OOH$ ($\dot{Q}OOH = H_2O + C_{n-1}$aldehydes + $H\dot{C}O$)
16	addition reactions of $\dot{Q}OOH$ to O_2 to form $\dot{O}_2QOOH$ (O_2 + $\dot{Q}OOH = \dot{O}_2QOOH$) (including specific features of $\alpha\dot{Q}OOH$)
17	isomerization reactions of $\dot{O}_2QOOH$ to form $\dot{O}H$ and carbonyl hydroxyalkyl hydroperoxides (CHHP)
18	decompositions of carbonyl hydroxyalkyl hydroperoxides (CHHP) to form $\dot{O}H$ and other carbonyl radical species
19	decompositions of carbonyl hydroxyalkyl hydroperoxides through the Korcek mechanism to form smaller organic acids and aldehydes
20	H atom abstraction reactions on carbonyl hydroxyalkyl hydroperoxides and decompositions

[a]Adapted from ref 5.

previous developments[51−53] of the CRECK model attached. Rate coefficients for the *n*-hexenol isomers (unsaturated alcohols from *n*-hexanol oxidation) are based on analogy estimates from lower-molecular-weight enols (pentenol and butenol isomers). The kinetic subset for aldehydes pyrolysis and high- and low-temperature oxidation has been recently developed as discussed by Pelucchi et al.[21−23] The consumption of intermediates such as epoxy alcohols (heterocyclic alcohols) via H atom abstraction reactions is treated as described elsewhere.[73] The general kinetic scheme for the pyrolysis and oxidation of alcohols is summarized in Figure 3. The kinetics adopted for the 20 reaction classes of Table 1 is described in detail below.

2.2. Unimolecular Initiation Reactions (Reaction Class 1). Unimolecular initiation reactions involving a C−C, C−O, C−H, or O−H bond fission are responsible for the initiation of the radical chain mechanism, in particular for pyrolysis and high-temperature-oxidation conditions. For this reaction class, the BDEs correspond to the activation energies of the elementary steps producing two radicals from the alcohol molecule. Indeed, the reverse radical−radical recombination reaction does not involve any energy barrier. From Figure 2, it is already possible to highlight the most favored initiation reactions, i.e., those involving the lower BDE. The C_α−C_β bonds are the weakest, with activation energies on the order of ∼86 kcal mol^{-1}. The alcohol-specific C−O bond connecting the carbon chain to the hydroxyl moiety (−OH) is the strongest, thus providing only a minor contribution to radical chain initiation. Figure 4 compares

https://dx.doi.org/10.1021/acs.energyfuels.0c02251
Energy Fuels 2020, 34, 14688−14707

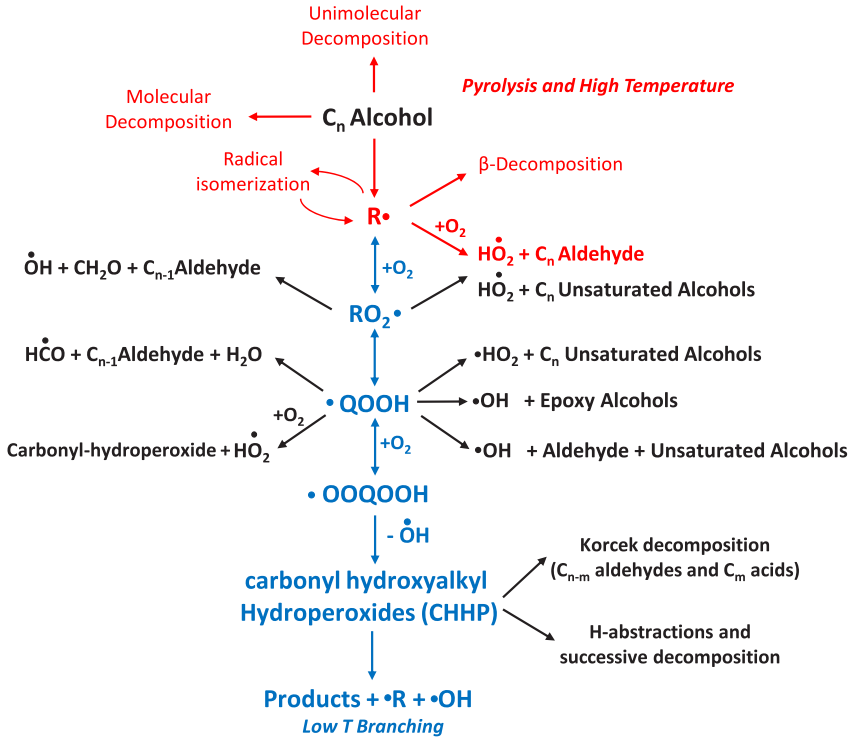

Figure 3. Simplified kinetic scheme for the pyrolysis, as well as high- and low-temperature oxidation, of linear alcohols.

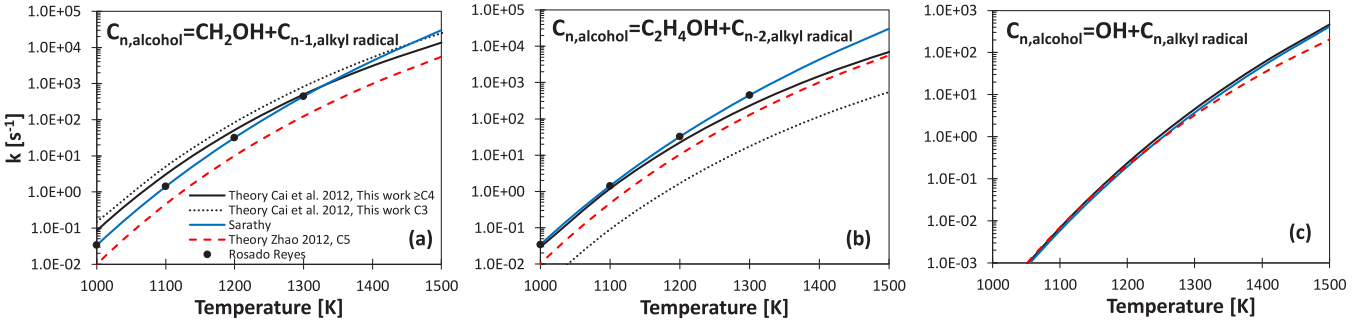

Figure 4. Comparison between unimolecular initiation rate constants involving the fission of C_α−O, C_α−C_β, and C_β−C_γ bonds at p = 1 atm. Symbols represent experimental data reported by Rosado-Reyes et al.[82] Dotted black lines represent data reported by Cai et al.[84] and adopted in this work for *n*-propanol, solid black lines represent data reported by Cai et al.[83] and adopted in this work for ≥*n*-butanol, solid blue lines represent data reported by Sarathy et al.[5] (*n*-butanol), and dashed red lines represent data reported by Zhao et al.[78] (*n*-pentanol).

values from the literature[5,78,82,83] with the rate constants adopted in this study for the unimolecular initiation reactions involving the fission of C−O (i.e., $C_n$alcohol = $\dot{O}H$ + $\dot{C}_n$ alkyl radical), C_α−C_β (i.e., C_n alcohol = $\dot{C}H_2OH$ + $\dot{C}_{n-1}$ alkyl radical) and C_β−C_γ (i.e., $C_n$alcohol = $\dot{C}_2H_4OH$ + $\dot{C}_{n-2}$ alkyl radical), at p = 1 atm.

Rosado-Reyes et al.[82] experimentally investigated the unimolecular decomposition of *n*-butanol in a single pulse shock tube (ST), at p = =1.5−6.2 bar and T = 1120−1250 K, providing fits with an uncertainty of ∼3 kcal mol^{-1}, corresponding to a factor of ∼3−4 in the temperature range of the measurements. Zhao et al.[78] presented a theoretical investigation of *n*-pentanol decomposition at the CBS-QB3 level of theory. The variational implementation of the transition state theory (VTST) was applied to determine the high-pressure-limit rate constants for barrier-less reactions, and the pressure dependence determined with RRKM/master equation simulations. Rate constants were provided for the temperature range of T = 800−2000 K. Similarly, Cai et al.[83,84] calculated pressure- and temperature-dependent rate constants for a series of butanol isomers, including *n*-butanol (1-butanol) and 2-butanol, at the CBS-APNO level of theory. According to the authors, inaccuracies as large as a factor of ∼2−3 are expected from the theoretical methods applied.

As in the kinetic model of Li et al.,[54] for the C_α−C_β decomposition channel (Figure 4a) in *n*-propanol, we adopt the rate constants for the reaction 2-butanol = $\dot{C}_2H_5$ + $CH_3\dot{C}HOH$, calculated by Cai et al.,[84] based on similarities between BDEs, as discussed by Man et al.[75] The same analogy applies to the decomposition reactions involving C_β−C_γ (Figure 4b), for which we adopted the analogous rate constant for the reaction 2-butanol = $\dot{C}H_3$ + $\dot{C}H_2CH(OH)CH_3$. This choice was made based on improved agreement obtained with pyrolysis experiments discussed in Section 4 and in Part II.[56]

For higher-molecular-weight alcohols ($C_n \geq 4$), we adopt the entire set of rate constants calculated by Cai et al.[83] for *n*-butanol. Concerning the C−O bond breaking channel (C_n alcohols = $\dot{O}H$ + $\dot{C}_n$ alkyl radical, Figure 4c), we adopt the

https://dx.doi.org/10.1021/acs.energyfuels.0c02251
Energy Fuels 2020, 34, 14688−14707

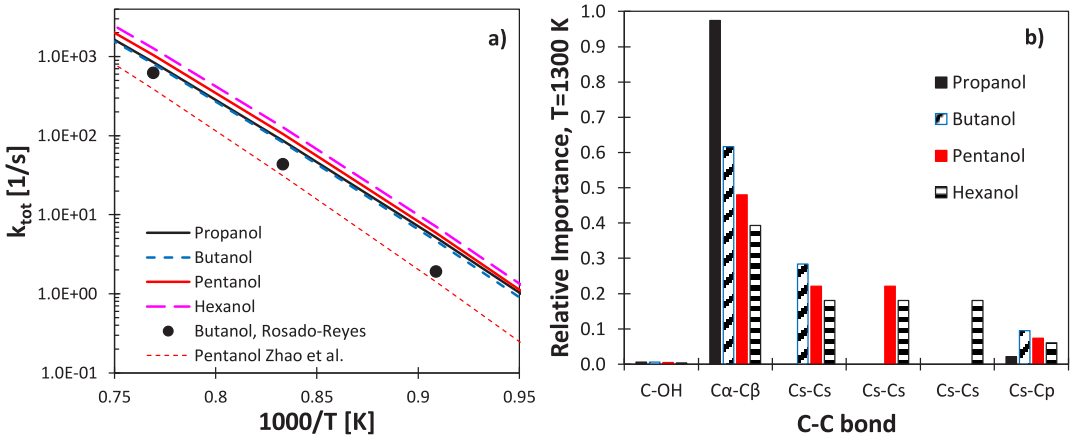

Figure 5. (a) Total decomposition rate constant for n-C_3−C_6 alcohols obtained from the rate constant values adopted in this work, compared with literature values.[78,82] (b) Relative importance of the different unimolecular decomposition channels.

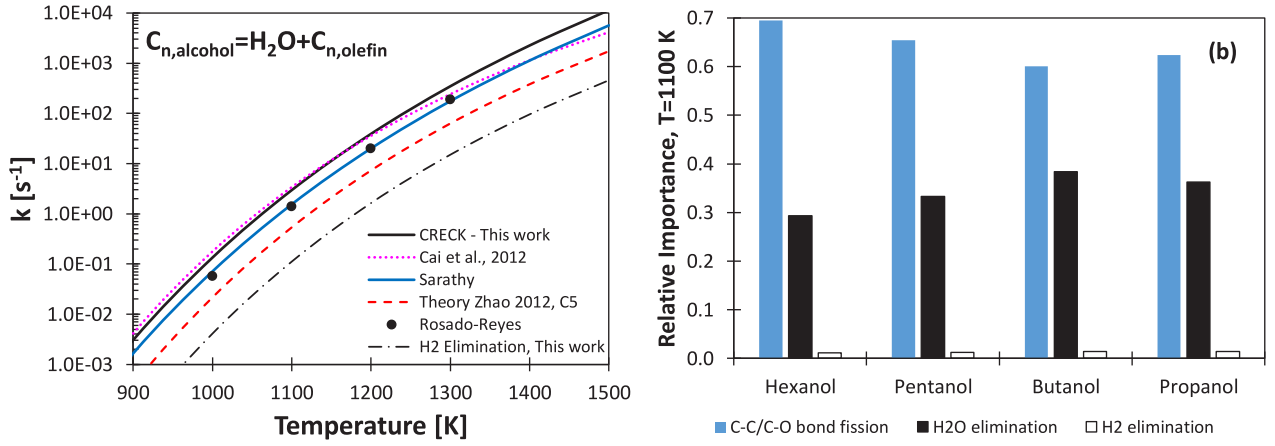

Figure 6. (a) Comparison between rate constants for four-centered molecular dehydration reaction from different sources.[5,78,82,83] (b) Relative contribution of four centered molecular reactions to the total unimolecular decomposition rate of n-C_3−C_6 alcohols.

values proposed by Li et al.[54] which is consistent with that suggested by Zhao et al.[78] No determination of this decomposition pathway was in fact provided in the experimental[82] and theoretical studies[83,84] mentioned above.

Generally, the set of values selected in the present work agrees with the results reported by Rosado-Reyes et al.,[82] within the reported uncertainties. Larger deviations, up to a factor of ≈5, are highlighted for the dominating C_α−C_β channel with respect to the determination of Zhao et al.[78] for n-pentanol.

Figure 5a shows the total decomposition rate constants for n-C_3−C_6 alcohols obtained as the sum of the unimolecular decomposition channels involving C−C and C−O bond fission. Aiming to highlight inconsistencies still existing in the literature on alcohols pyrolysis and combustion, it should be observed that n-propanol shows a total rate of decomposition ∼20% higher than that of n-butanol, in disagreement with the expected increase of total decomposition rates from bond fission reactions with increasing carbon chain length. Figure 5b compares the relative importance of the different unimolecular decomposition channels, highlighting its correlation with BDEs (C−OH, ∼94 kcal mol^{-1} < Cs−Cp, ∼89 kcal mol^{-1} < Cs−Cs, ∼88 kcal mol^{-1} < C_α−C_β, ∼86 kcal mol^{-1}). The decomposition reaction C_n alcohol = $\dot{C}H_2OH$ + $\dot{C}_{n-1}$ alkyl radical play a major role, covering ∼97% in n-propanol, versus ∼43% in n-hexanol. Despite the selected rate parameters showing good agreement with the pyrolysis experiments, it is worth underlining the need of a systematic theoretical investigation of unimolecular initiation reactions to reconcile the inconsistent information available in the literature.

Reaction pathways involving the breaking of C−H or O−H bonds generally provide a negligible contribution to the unimolecular decomposition of the fuel molecule. The same reference kinetic parameter is adopted for the reverse recombination reaction (k = 5.0 × 10^{13} cm^3 mol^{-1} s^{-1}). Rate parameters for these reactions in the reverse decomposition direction are consistent with the BDEs of C−H and O−H bonds discussed at the beginning of Section 2.

2.3. Four-Centered Molecular Decomposition Reactions: Dehydration and Dehydrogenation (Reaction Class 2). This class of reactions proceeds through a four-center cyclic transition state, forming the parent alkenes and H_2O. Figure 6a compares the rate constants adopted in this work at p = 1 atm with the values proposed in previous studies.[5,78,82,83] The proposed values agree within a factor of 2 with the values proposed by Sarathy et al.,[5] Cai et al.,[83] and Rosado-Reyes et al.[82] The rate constant from Zhao et al.[78] is ∼6 times lower.

Four-centered molecular dehydrogenation producing the parent aldehyde can also occur as discussed in Grana et al.[52] and Nativel et al.[53] for n-butanol and n-pentanol, respectively. Rate constants are adopted based on the analogy with the same reaction in n-alkanes,[85] and their contribution is much lower (∼30 times), compared to dehydration.

https://dx.doi.org/10.1021/acs.energyfuels.0c02251
Energy Fuels 2020, 34, 14688−14707

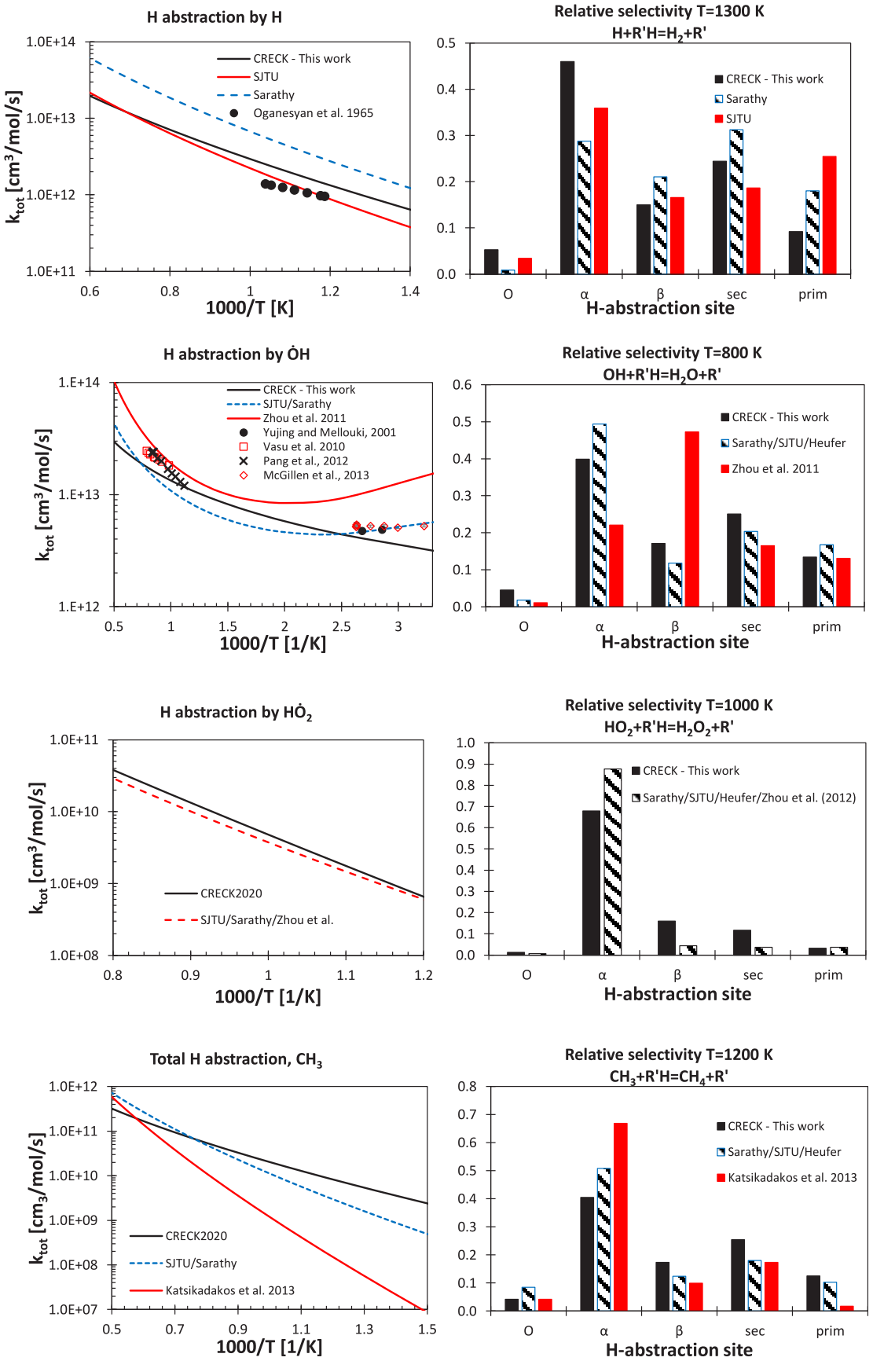

Figure 7. (Left) Total rate constants of H-atom abstraction reactions by Ḣ, ȮH, HȮ$_2$, and ĊH$_3$ on *n*-butanol from this work (black) and from the literature.[5,41−45,48,49,83,87] (Right) Relative selectivity to the different H-atom abstraction site for *n*-butanol from this work (black) and from the literature.

https://dx.doi.org/10.1021/acs.energyfuels.0c02251
Energy Fuels 2020, 34, 14688−14707

Table 2. Rate Coefficients for Alcohol Radical Isomerization and Decomposition Reactions[a]

n-butanol radicals	A [s^{-1}]	n	E_a [cal mol^{-1}]	ref	notes
		$R_n\dot{O}$			
↔ CH_2O + $\dot{C}_{n-1}$ Alkyl Radical	6.0×10^{13}	0.00	15000.	52	A/0.5[b]
↔ $\dot{H}$ + C_n Aldehyde	1.0×10^{13}	0.00	26000.	52	A/3[b]
		$\dot{R}_n\alpha$			
↔ $\dot{H}$ + C_n Aldehyde	3.0×10^{13}	0.00	38000.	52	E_a = +1 kcal/mol[c]
↔ C_2H_3OH + $\dot{C}_{n-2}$ Alkyl Radical	1.0×10^{13}	0.00	28000.	52	
↔ $\dot{H}$ + C_n Enol	1.0×10^{13}	0.00	38000.	52	
		$\dot{R}_n\beta$			
↔ $\dot{O}H$ + C_n Alkene	7.2×10^{42}	−9.04	37600.	83	
↔ C_3H_5OH + $\dot{C}_{n-3}$ Alkyl Radical	5.0×10^{12}	0.00	27000.	83	
↔ $\dot{H}$ + C_n Enol	1.0×10^{13}	0.00	34000.	52	
↔ $\dot{H}$ + C_n Aldehyde	3.0×10^{13}	0.00	38000.	52	E_a = +1 kcal/mol[c]
↔ *RO̊ (4-membered ring)*	5.0×10^{11}	0.00	26000.	52	
		$\dot{R}_n$sec			
↔ CH_2OH + C_{n-1} Alkene	6.0×10^{13}	0.00	31000.	52	A/0.5, E_a = +1 kcal/mol[d]
↔ $\dot{H}$ + C_n Enol	3.0×10^{13}	0.00	38000.	52	E_a = +1 kcal/mol[c]
↔ *RO̊ (5-membered ring)*	1.0×10^{11}	0.00	23000.	52	
↔ C_2H_4+ $\dot{C}H_2(CH_2)_{n-3}OH$	3.0×10^{13}	0.00	30000.	52	
		$\dot{R}_n$prim			
↔ $\dot{H}$ + C_n Enol	2.0×10^{13}	0.00	37000.	52	A/1.5, E_a = +1 kcal/mol[c]
↔ *RO̊ (6-membered ring)*	1.6×10^{10}	0.00	16000.	52	
↔ *Rȯα (5-membered ring)*	2.0×10^{11}	0.00	19600.	52	

[a]The same rate rules are adopted to describe the decomposition of radicals for the series *n*-C_3−C_6 alcohols. Modifications to the pre-exponential factors (A) or to the activation energies (E_a), with respect to Grana et al.,[52] are provided. [b]For improved agreement in speciation data prediction at high temperatures for CH_2O and C_n aldehyde. [c]For better agreement with rate constant suggestion from Sarathy et al.[5] [d]For better agreement with theoretical determination by Zhang et al.[88]

Figure 6b shows the relative contributions of four-centered molecular reactions and bond fission reactions to the unimolecular decomposition of *n*-C_3−C_6 alcohols at T = 1100 K and p = 1 atm, confirming the negligible role of the dehydrogenation channel. The dehydration reaction, for which we adopted the same rate parameters for the full series of alcohols, because the reactions proceed through analogous four-centered transition states, contributes ∼30%−40% to the total decomposition rate constant. As expected, the relative weight decreases for increasing molecular weight, with the exception of *n*-propanol. This deviation is related to the different set of unimolecular decomposition reactions adopted for *n*-propanol, as discussed in Section 2.2.

2.4. H-Atom Abstraction Reactions (Reaction Class 3). Rate parameters of H atom abstraction reactions are determined according to the systematic approach described by Ranzi et al.[86] Regarding the alkane-like moiety of *n*-C_3−C_6 alcohols, primary and secondary sites are treated according to alkane rules for analogous H atom abstraction sites in the general form of $\dot{R}$ + R′H = RH + $\dot{R}$′, where R′H is a fuel molecule and $\dot{R}$ is a generic abstracting radical. To account for the stronger BDE for the C_β−H bond, the reference values adopted for alkane-like secondary sites have been decreased by 25%. Kinetic parameters for the weakened secondary C_α−H bond have been obtained by increasing the reference rate constants by 75%. From the following discussions, such modifications are well within the expected uncertainty of theoretical and experimental determinations available for the most important abstracting radicals: $\dot{H}$, $\dot{O}H$, $H\dot{O}_2$, $\dot{C}H_3$. The same reference parameters have been applied to the entire alcohol series. Such reference parameters are reported in Table S3 in the Supporting Information.

Figure 7 compares the total rate constants of H-atom abstraction from *n*-butanol by $\dot{H}$, $\dot{O}H$, $H\dot{O}_2$, and $\dot{C}H_3$ implemented in the kinetic model attached to this work with those from previous theoretical,[41−43] experimental,[44,45,48,49,87] and kinetic modeling studies.[5,83] Regarding H-atom abstraction by $\dot{H}$ atoms, our total rate constant agrees with the experimental determination by Oganesyan et al.[87] and with Cai et al.,[83] within a factor of ∼2. Sarathy et al.[5] proposed a value that was ∼3 times higher than the estimate by Cai et al.[83] In terms of selectivity to the available H-atom abstraction sites (O, α, β, secondary, and primary) at T = 1300 K, trends are as expected from the BDEs (Figure 2) and from the number of available H atoms. Abstraction from the α-site is the most favored channel, followed by the secondary position of the alkane-like moiety, β, the terminal primary position, and the H-atom abstraction from the hydroxyl substitution. The selectivities from the kinetic model attached to this study are 46%, 25%, 15%, 9%, and 5%. Zhou et al.[43] presented the only theoretical determination of H-atom abstraction reactions by $\dot{O}H$ from *n*-butanol over the entire temperature range of interest for pyrolysis and combustion applications (T = 500−2000 K). The total rate constant by Zhou et al. agrees with the higher temperature (T > 900 K) experimental determinations[45,49] within a factor of 1.5, while larger deviations exist in comparison with lower temperature data.[44,48] Our proposed rate constant agrees with the experimental data and with the values adopted in refs 5 and 83, within a factor of ∼2. The calculations by Zhou et al.[43] show an unexpected dominant role of the H-atom abstraction from the β-position, in evident disagreement with previously validated kinetic models. Better agreement, in terms of relative selectivities at T = 800 K, is observed between our set of rate constants and those adopted in refs 5 and 83. In particular, the dominating channel is once again α (40%), followed by the alkane-like secondary position (25%), β (17%), primary site (13%), and the hydroxyl moiety (5%).

https://dx.doi.org/10.1021/acs.energyfuels.0c02251
Energy Fuels 2020, 34, 14688−14707

The rate constant of H-atom abstraction by $H\dot{O}_2$ adopted in our work agrees within 20% with the calculations of Zhou et al.,[41] in terms of absolute rate. This agreement was obtained by modifying the reference kinetic parameters discussed at the beginning of this section, through a global increase of a factor of 8.4. The *n*-butanol models of Sarathy et al.[5] and Cai et al.[83] adopt the theoretical values of Zhou et al.[41] for the single channels. In terms of relative importance, this set of rate constants results in a very high selectivity (i.e., 88% at T = 1000 K), in favor of the α-site. According to our systematic analysis presented here and to previous modeling efforts[20,51−53,56] a more realistic selectivity (O = 1%, α = 68%, β = 16%, secondary = 12%, primary = 3%) was obtained distributing the increase of the absolute rate (i.e., a factor of 8.4) by multiplying the reference parameters by 3.5 for α, 2 for β and 1.2 for the hydroxyl moiety. In fact, the impact of the high selectivity toward the α-position proposed by Zhou et al.[41] would significantly worsen model predictions.

Katsikadakos et al.[42] calculated rate constants for the H-atom abstraction reactions by methyl radical ($\dot{C}H_3$) from *n*-butanol. Reasonable agreement, i.e., a factor of <3, with our rate constants and those from Sarathy et al.[5] and Cai et al.[83] is observed only for T > 1350 K. At lower temperatures, deviations as large as 3 orders of magnitude are highlighted. Taking advantage of a very significant number of pyrolysis data,[37,54,55,59,84] where the H-atom abstractions by $\dot{C}H_3$ play a significant role for the validation of our model, we observed negative effects on model performances when implementing the theoretical values. Moreover, our reference kinetic parameters were found to agree quite satisfactorily (by a factor of <3) with the estimates reported in refs 5 and 83, both in terms of absolute rate constant and relative selectivities, as reported in Figure 7. Also, for H atom abstraction by methyl radical, the dominating channel is once again α (40%), followed by the alkane-like secondary position (25%), the secondary β site (17%), the terminal primary site (13%), and the hydroxyl moiety (5%).

2.5. Decomposition and Isomerization Reactions of Alcohol Radicals. (Reaction Classes 4 and 5). At high temperatures (e.g., T > 900 K), fuel radicals can decompose via β-scission reactions, or isomerize through internal hydrogen abstractions proceeding through a cyclic transition state.

Table 2 shows the reference rate parameters adopted in the kinetic model discussed here, taking *n*-butanol as an example. The selected values were adopted from our previous kinetics studies,[51−53] with some minor adjustments, based on our literature review and on the comprehensive model validation summarized in Section 4 and discussed in Part II of this study.[56] The same rate rules are systematically applied to the entire *n*-C_3−C_6 alcohol series. The rate constants are compared with those proposed in the review by Sarathy et al.[5] in Figure S1 in the Supporting Information.

Alkoxy radicals ($R_n\dot{O}$) mostly decompose and produce formaldehyde (CH_2O) and a $\dot{C}_{n-1}$ primary radical (e.g., *n*-propyl radical). Alkoxy radicals are generally very reactive, compared to primary and secondary alkyl radicals, as expected from the high BDE of the O−H bond. As a result, the decomposition of alkoxy radicals ($R\dot{O}$) are approximately an order of magnitude faster, compared to the β-decomposition of the other alkyl radicals described in the following. An additional pathway leads to the fission of the C_α−H bond located at the β-position to the unpaired electron producing $\dot{H}$ atoms and the parent C_n aldehyde (e.g., *n*-butanal). Compared to similar reactions in alkanes, this latter step is particularly favored for alcohols, because of the lower BDE of C_α−H, but is still of much lower importance, compared to β-scissions involving a C−C bond.

The secondary radical $\dot{R}\alpha$ largely decomposes forming ethanol (C_2H_3OH) and a $\dot{C}_{n-2}$ primary radical (e.g., ethyl radical). The rate constant for this reaction is over an order of magnitude higher than the two other possible β-scission reactions involving the breaking of a C−H bond, forming a C_n unsaturated alcohol (*n*-butenol), or an O−H bond. This latter pathway leads to the formation of the parent C_n aldehyde.

The decomposition of the secondary radical in the β-position primarily leads to the formation of the parent C_n 1-olefin by C−O bond cleavage, thus releasing $\dot{O}H$ radicals. An additional important decomposition route is in the formation of 2-propenol (C_3H_5OH) and a $\dot{C}_{n-3}$ alkyl radical (e.g., methyl radical). Another available minor pathways produce $\dot{H}$ atoms and C_n enols or aldehydes. Aiming for a compact subset of reactions to describe alcohols pyrolysis and oxidation, we only consider one representative lumped C_n enol formed from the decomposition of *n*-C_3−C_6 alcohol radicals.

Secondary radicals of the alkane-like moiety mainly decompose and form hydroxymethylene radical ($\dot{C}H_2OH$) and a C_{n-1} alkene (e.g., propene). For alcohols heavier than *n*-butanol, an additional pathway forming 3-butenol (C_4H_7OH) and a $\dot{C}_{n-4}$ alkyl radical is available. Rate constants for this latter channel are estimated by analogy with β-scission reactions of secondary alkyl radicals.[74] Primary radicals largely decompose to form ethylene (C_2H_4) and the primary radical of a $\dot{C}_{n-2}$ alcohol (e.g., $\dot{C}_2H_4OH$). Even for these last cases, the dehydrogenation channels are less favored under the conditions of interest (T = 500−2000 K).

Isomerization reactions of alcohols radicals are explained on the basis of internal H atom abstraction reactions, via 5-membered, 6-membered, and 7-membered ring intermediates. The rate constants of these isomerization reactions are estimated, in terms of the number of atoms in the transition state ring structure (including the H atom) and the type of sites involved in the H atom transfer.[89] To this aim, the rates are also influenced by the different BDEs of the alcohol-specific moiety and must be taken into account, as discussed in the work of Nativel et al.[53] For this reason, we also consider 4-membered transition-state structures leading to the internal H-atom abstraction of the hydrogen of the weakest C_α−H bond.

2.6. Reactions of O_2 with Alcohols Radicals To Form $H\dot{O}_2$ and a C_n Aldehyde/Enol (Reaction Class 6). Stable C_n aldehydes and enols are formed at high temperatures through β-scission reactions involving the C−H bond. At lower temperatures, the same compounds can be formed by direct H-atom abstraction by O_2 forming an unsaturated bond and $H\dot{O}_2$ ($\dot{R}_n$ + O_2 = $H\dot{O}_2$ + R_n-aldehyde/enol). In particular, the reactions of primary and secondary radicals of the alkane-like moiety and of the secondary radicals in the β-position form the parent unsaturated alcohol. Rate constants for this reaction class have been adopted from similar reactions of alkane fuel combustion ($k = 3 \times 10^{11} \exp(-3500\ [\text{cal/mol}]/RT)\ [\text{cm}^3/\text{mol/s}]$). Reactions of α radicals with O_2 produce the parent aldehyde and $H\dot{O}_2$. Because of the high selectivity toward the formation of α-radicals through H-atom abstraction reactions (see Section 2.3), this latter pathway has a high impact on alcohol reactivity and largely justifies, from a purely chemical kinetic perspective, the high octane rating of alcohol fuels. Indeed, only radicals in the β-position and in the alkane-like moiety effectively undergo addition to O_2, forming the peroxy radical and activating the branching pathways responsible for low-temperature reactivity.

https://dx.doi.org/10.1021/acs.energyfuels.0c02251
Energy Fuels 2020, 34, 14688−14707

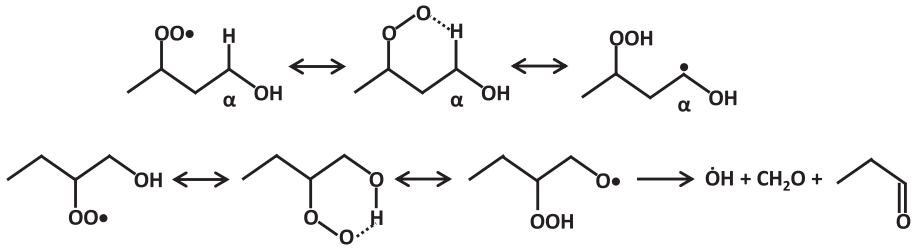

Figure 8. Example 6-membered isomerization reactions in *n*-butanol oxidation. The top row shows sec-$R\dot{O}_2$ producing α-$\dot{Q}OOH$; the bottom row shows (Waddington mechanism): β-$R\dot{O}_2$ producing an hydroperoxy alkoxyradical and its successive decomposition.

Despite a more systematic theoretical evaluation of $\dot{R}\alpha + O_2$ for a series of alcohols would be necessary in order to obtain more-accurate rate rules, the high-pressure-limit rate constant computed by Zádor et al.[38] has been adopted for $\dot{R}_n\alpha + O_2 = H\dot{O}_2 + C_n$ aldehyde. According to Zádor et al.,[38] the concerted elimination reaction yielding aldehyde and $H\dot{O}_2$ proceeds through the formation of an aldehyde−HO_2 complex, rapidly decomposing to the products.

2.7. Addition Reactions of Alcohol Radicals to O_2 ($\dot{R} + O_2 = R\dot{O}_2$) (Reaction Class 7). Similarly to alkanes, the transition between high- and low-temperature regimes is dependent on the competition between β-scission reactions of alcohol radicals (Section 2.4) and their addition to O_2, forming hydroxyalkyl-peroxy radicals ($R\dot{O}_2$). Although this step does not directly determine the rate of chain branching, the correct description of the relative concentrations of alkyl and peroxyl radicals is a necessary condition to fully characterize low-temperature ignition phenomena. As reviewed by Sarathy et al.[5] no specific theoretical studies have been dedicated to a comprehensive assessment of alcohol-specific rate constants for this reaction class; therefore, we base our reference rate parameters for alcohol fuels on the rate rules provided by Ranzi et al.[90] for alkanes. In particular, we adopt a value of 1.0×10^{12} $cm^3\ mol^{-1}\ s^{-1}$ for the primary radicals and a value of 2.0×10^{12} $cm^3\ mol^{-1}\ s^{-1}$ for secondary radicals, including β (see Table 3). We assume that $\dot{R}_n\alpha$ radical does not undergo addition to O_2. Indeed, as reported in the theoretical studies for ethanol by Zádor et al.[38] and da Silva et al.,[31,32] under the conditions of interest for combustion applications, the peroxy radical obtained from such an addition reaction would rapidly dissociate back to the reactant, favoring the direct pathway to $H\dot{O}_2$ and the parent aldehyde.

2.8. Recombination/Disproportionation Reactions of $R\dot{O}_2$ Radicals: $R\dot{O}_2 + R'\dot{O}_2$ and $\dot{R} + R'\dot{O}_2$ ($\dot{R}'$ = H, $\dot{C}H_3$, Alcohol Radicals) (Reaction Classes 8 and 9). $R\dot{O}_2$ radicals can undergo recombination/disproportionation reactions forming $R\dot{O}$ and $R'\dot{O}$ radicals. The recombination of hydroxyalkyl-peroxy radicals ($R\dot{O}_2 + R'\dot{O}_2$) produces O_2 and a $ROOR'$ intermediate that rapidly decomposes to two alkoxy radical $R\dot{O}$ and $R'\dot{O}$, whose decomposition rate is also very fast, by analogy with the $R\dot{O}$ radicals decomposition described in Section 2.4. Depending on the chain length of the fuel (C_nOH) on the nature of $\dot{R}'$ (H, $\dot{C}H_3$, alcohol radicals) and on the location of the peroxy radical moiety, $R\dot{O}$ and $R'\dot{O}$ decomposition products are C_m aldehydes of different molecular weight ($m < n$, formaldehyde, acetaldehyde, propanal, butanal, etc.), primary alkyl radicals of smaller alcohols ($\dot{C}H_2OH$, $\dot{C}H_2CH_2OH$, $\dot{C}H_2CH_2CH_2OH$, etc.), $\dot{O}H$, and $CH_3\dot{O}$. The recombination of fuel radicals $\dot{R}$ and $R'\dot{O}_2$ produces the same $R\dot{O}$ and $R'\dot{O}$ from the decomposition of the $ROOR'$ intermediate. Also, in this case, $R\dot{O}$ and $R'\dot{O}$ are assumed to directly decompose to the same products. Similar reactions for *n*-alkanes have been thoroughly discussed recently by Ranzi and co-workers,[73] from which we adopt the reference kinetic parameters (see Table 3).

2.9. $R\dot{O}_2$ Concerted Eliminations To Form $H\dot{O}_2$ + Aldehyde/Enol (Reaction Class 10). $R\dot{O}_2$ radicals can eliminate $H\dot{O}_2$, forming a C_n aldehyde or enol. The same reaction class produces $H\dot{O}_2$ and alkenes under low-temperature oxidation in *n*-alkanes. Reference rate parameters have been adopted from the review paper of Sarathy et al.[5] From a low temperature reactivity standpoint, this reaction directly competes with the isomerization of $R\dot{O}_2$ radicals described in the following section.

2.10. $R\dot{O}_2$ Isomerization Reactions ($R\dot{O}_2 \rightleftharpoons \dot{Q}OOH$), Including Waddington-Type Reactions ($R\dot{O}_2 = \dot{O}H + CH_2O + C_{n-1}$ Aldehyde) (Reaction Class 11). Intramolecular H-atom abstraction reaction of hydroxyalkyl-peroxy radicals ($R\dot{O}_2$) to form hydroperoxyl-alkylhydroxy radicals ($\dot{Q}OOH$) are the second step in the low-temperature chain branching pathway of alcohol oxidation (Figure 2). 5- and 6-membered isomerization reactions by tying up 3 and 4 internal rotors, respectively, are considered herein. As discussed previously,[73,74,79,90,91] the activation energy can be computed as $E_a = E^0_{ref,R} + EC_{R'H} + E_{rs}$, where $E^0_{ref,R}$ is the reference activation energy for a peroxyl radical abstracting a primary H atom (21.5 kcal mol^{-1}),[86] $EC_{R'H}$ is the correction to account for the type of H atom abstracted, based on the BDEs discussed in Section 2 (i.e., 0.0 kcal mol^{-1} for primary, −2.5 kcal mol^{-1} for secondary, −4.0 kcal mol^{-1} for α, +1.0 kcal mol^{-1} for β, +2 kcal mol^{-1} for OH) and E_{rs} is the ring strain energy (i.e., +1.0 kcal mol^{-1} for 6-membered, +7.0 kcal mol^{-1} for 5-membered). As an example, for the isomerization reaction reported in Figure 8, the activation energy is 18.5 kcal mol^{-1} in the forward direction.

The reference frequency factor is 2.0×10^{11} s^{-1} derived from the reference frequency factor for the internal H atom abstraction of one single primary hydrogen atom through a 6-membered transition state. Lowering the number of hindered internal rotors by one (e.g., in the case of a 5-membered isomerization) increases the frequency factor by $10^{0.8}$ s^{-1}, resulting in a reference pre-exponential factor of $10^{11.8}$ s^{-1}, and increases the activation energy by 6 kcal mol^{-1}. Reverse rate constants can also be estimated in a similar fashion as discussed in previous studies,[73,74,79,90,91] again, taking into account the relative stability of $\dot{Q}OOH$ radicals as retrieved from the bond dissociation energies (i.e., α-$\dot{Q}OOH$ > sec-$\dot{Q}OOH$ > β-$\dot{Q}OOH$ > prim-$\dot{Q}OOH$) of Section 2. Reference rate parameters for the $R\dot{O}_2 \rightleftharpoons \dot{Q}OOH$ isomerization reactions are reported in Table 3, presented later in this work.

β-$R\dot{O}_2$ radicals (C_n) can isomerize to transfer the H atom of the hydroxyl moiety to form alkoxy hydroperoxy radicals, which rapidly decompose to form formaldehyde, C_{n-1} aldehyde, and

https://dx.doi.org/10.1021/acs.energyfuels.0c02251
Energy Fuels 2020, 34, 14688−14707

$\dot{O}H$ ($R\dot{O}_2$ = $\dot{O}H$ + CH_2O + C_{n-1} aldehyde). This specific reaction is known as the Waddington mechanism.[92] The associated reference rate parameters adopted from Sarathy et al.[5] in our previous kinetic modeling studies of alcohol low-temperature oxidation[17,20] have been corrected according to the recent theoretical study by Li et al.[93] The reference kinetic parameters were increased by a factor of 6 (see Table 3, presented later in this work), agreeing within a factor of 2 with the recent theoretical calculation.

2.11. $\dot{Q}OOH$ Radical Decomposition Reactions (Reaction Classes 12−15). The low-temperature branching pathway can be inhibited by the occurrence of unimolecular decomposition reactions of $\dot{Q}OOH$ radicals. If the radical site is located γ to the hydroperoxy function (−OOH) β-scission reactions forming an alkene (or an enol) and a carbonyl compound (aldehydes, hydroxyl aldehydes), together with $\dot{O}H$ radical occur. $\dot{Q}OOH$ radicals with the radical site located β to the OOH group decompose to form $H\dot{O}_2$ and a C_n enol. Reference rate parameters are taken based on the analogy with *n*-alkanes[73,74,79,90,91] (see Table 3, presented later in this work). By analogy to cyclic ether formation in the oxidation of alkanes, cyclization reactions produce epoxy alcohols and an $\dot{O}H$ radical. Once again, the energy barrier and the frequency factor are dependent on the size of the cyclic species formed. Specifically, an activation energy of 18 kcal mol^{-1} is assumed for the formation of oxirane alcohols (3-membered cyclic ether moiety); this decreases to 17 kcal mol^{-1} for oxetane alcohols (4-membered cyclic ether moiety) and to 8.5 kcal mol^{-1} for epoxy alcohols with a 5-membered cyclic ether moiety. The frequency factor ranges from 10^{12} s^{-1} to $10^{10.4}$ s^{-1}, depending on the number of rotors tied up. H-atom abstraction reactions are considered to take into account the consumption of epoxy alcohols. Rate constants are based on analogy with H-atom abstraction reactions on cyclic ethers in alkanes.[73,74,79,90,91]

In addition to alkane-like decomposition reactions, Welz et al.[40] proposed and investigated an unconventional dehydration pathway of α-$\dot{Q}OOH$ radicals occurring in alcohol oxidation (Figure 9). The rate constant is estimated in this work by taking

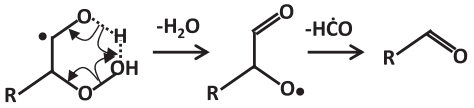

Figure 9. Dehydration channel of $\dot{Q}OOH$ radicals[40] and successive decomposition.

into account the formation of a cyclic transition state and the calculated energy barrier (~13 kcal mol^{-1}). In addition to water, these reactions produce a C_{n-1} aldehyde and a formyl radical ($H\dot{C}O$).

2.12. $\dot{Q}OOH$ Radicals Addition to O_2 ($\dot{Q}OOH$ + O_2 = $\dot{O}_2QOOH$) (Reaction Class 16). The third step in the low-temperature chain-branching pathway involves a second addition to O_2 to form $\dot{O}_2QOOH$ radicals. Rate constants are taken in analogy with the first addition $\dot{R}$ + O_2 = $R\dot{O}_2$ and are dependent on the nature of the radical site. If the radical site is located in α (α-hydroxy-hydroperoxyalkyl radical), its interaction with O_2 directly leads to the formation of a carbonyl-hydroperoxide (e.g., hydroperoxy butanal) and $H\dot{O}_2$. An example of this peculiar reaction is represented in Figure 10. Rate constants are taken in analogy with the $\dot{R}_\alpha$ + O_2 reaction (reaction class 6) investigated by Zádor et al.[38] The consumption pathways of the carbonyl-hydroperoxide species

Figure 10. α-Hydroxy-hydroperoxyalkyl radical and its interactions with O_2 to form a carbonyl-hydroperoxide (e.g., hydroperoxy butanal) and $H\dot{O}_2$.

thus obtained are already described in the subset of the CRECK model describing the consumption of ketohydroperoxides formed in *n*-alkane oxidation (e.g., *n*-butane).

2.13. Isomerization Reactions of $\dot{O}_2QOOH$ To Form $\dot{O}H$ and a Carbonyl Hydroxyalkyl Hydroperoxide (Reaction Class 17). The same rate rules described for the first isomerization ($R\dot{O}_2$ ⇌ $\dot{Q}OOH$, reaction class 11) are adopted to describe the second isomerization leading to the formation of $\dot{O}H$ and a carbonyl alkyl hydroperoxide. As in the description of alkanes low-temperature branching pathways in the CRECK kinetic model, these reactions are considered in the lumped form, directly eliminating $\dot{O}H$ and neglecting the formation of the intermediate that is rapidly decomposed (Figure 11).

2.14. Decomposition of Carbonyl Hydroxyalkyl Hydroperoxides To Form Oxygenated Radical Species, $\dot{O}H$, and Carbonyl Compounds (Reaction Class 18). The last step of the low-temperature branching pathway leads to the formation of oxygenated radical species and stable molecules, together with an $\dot{O}H$ radical. The rate-limiting event in this decomposition reaction is the fission of the O−OH bond of the hydroperoxyl functional group; successive β-scission reactions are responsible for the formation of the oxygenated products. Reference rate parameters are reported in Table 3, presented later in this work. Figure 12 shows an example of *n*-butanol carbonyl hydroxyalkyl hydroperoxides (CHHP) decomposition reactions.

2.15. Decomposition of Carbonyl Hydroxyalkyl Hydroperoxides through the Korcek Mechanism and H-Atom Abstraction Reactions. Ranzi et al.[73] recently proposed additional consumption pathways for ketohydroperoxides in *n*-alkanes, which directly compete with the branching decomposition of ketohydroperoxides at very low temperatures and relatively high fuel concentration, inhibiting reactivity. For completeness, the same alternative channels are considered herein for the decomposition of carbonyl alkyl hydroperoxides, despite their negligible impact on overall low-temperature reactivity for the available targets (see Section 4 and Part II of this study[56]).

Korcek-type mechanisms produce aldehydes or carbonyl compounds and organic acids (e.g., formic and acetic acids) (Figure 13), while H-atom abstraction reactions and successive β-scissions produce hydroxyl diones. Successive reactions of formic and acetic acids are already described in the core chemistry of the CRECK kinetic model. For simplicity, and because of the lack of experimental evidence on the formation of such species (i.e., hydroxyl diones), we consider them to have been directly decomposed to stable molecules, to respect the atomic balance.

To conclude Section 2, Table 3 provides a synoptic view of reference kinetic parameters to describe the low-temperature oxidation of alcohols.

3. LUMPING OF THE DETAILED KINETIC MECHANISM

Simplification of detailed kinetic mechanisms through lumping techniques allows the description of complex reactive systems

https://dx.doi.org/10.1021/acs.energyfuels.0c02251
Energy Fuels 2020, 34, 14688−14707

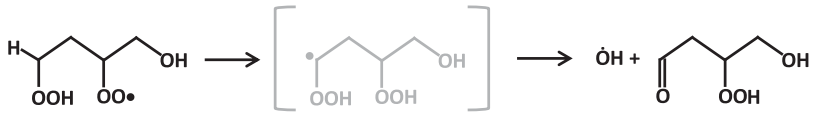

Figure 11. Example of a 6-membered second isomerization reaction directly forming OH and a carbonyl alkyl hydroperoxide. The intermediate species in gray is neglected in the kinetic model.

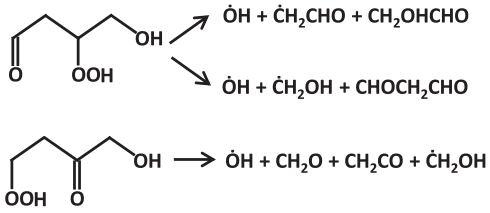

Figure 12. Example of CHHP branching decomposition reactions.

with a relatively limited number of species and reactions. Dente, Ranzi, and co-workers[90,91,94] described in detail the assumptions and the algorithms underlying the application of lumping. The same techniques extensively adopted for conventional hydrocarbon fuels (e.g., *n*-alkanes, cycloalkanes, *iso*-alkanes, aromatics) also have been successfully applied recently to a wide range of oxygenated fuels,[20−23,27,51−53] including alcohols. The main issues to be tackled when applying lumping techniques are (1) define which species must be lumped, (2) determine how the species to be lumped contribute to the final lumped species, and (3) determine lumped reactions and kinetic parameters. All of the above stem from the knowledge of the detailed chemistry that is occurring, motivating physically meaningful choices and supporting unavoidable assumptions. Clearly, depending on the extent of the simplifications applied, some level of detail can be lost; however, in the eventuality of experimental evidence shedding light on the formation of specific intermediates and products in significant quantities, the reversibility of lumping can be exploited, to increase the level of detail. However, the approach of Ranzi et al.[90] aims at reducing the number of species involved in the kinetic model while retaining very good predictive capabilities. In particular, these simplifications are of utmost convenience and importance when aiming at the development of a single kinetic model to describe the pyrolysis and oxidation of fuels from hydrogen to heavy fuel oils, including biofuels and bio-oils, as well as the formation of pollutant such as NOx and particulate matter. This is the overarching goal of the CRECK kinetic framework.[62]

A detailed description of fuel radicals is retained for *n*-propanol (primary (γ, β, α) and alkoxy (RȮ) radicals) and *n*-butanol (primary (δ), secondary (γ, β, α), and alkoxy (RȮ) radicals), to preserve consistency with the kinetic subsets of other isomer structures developed in previous kinetic studies.[51,52] Alkoxy radicals (RȮ) for higher-molecular-weight alcohols are assumed to be directly decomposed to their main β-scission products ($R_nȮ \leftrightarrow CH_2O + Ċ_{n-1}$ alkyl radical). The assumption is based on the high decomposition rate ($10^8 - 10^{12}$ s^{-1}, T = 500−2000 K) of alkoxy radicals, compared to β-decomposition reactions of alkyl radicals ($10^2 - 10^{10}$ s^{-1}), on the negligibility of interactions with O_2, leading to low-temperature chain branching, and on the relatively low selectivity of H-atom abstraction reactions to RȮ (<8% for T = 500−2000 K) (see Figure S1 in the Supporting Information). Only two fuel radicals are introduced for *n*-pentanol and *n*-hexanol: one representing the alcohol-specific α-radical (A) and one representing the alkane moiety (B). Rate constants for H-atom abstraction reactions from the α-site forming radical (A) are assigned as described in Section 2.3, and its successive decomposition reactions are as described in Table 2.

Rate constants of H-atom abstraction reactions on the remaining sites leading to the formation of radical (B) are given by the sum $k_{abs,B} = \sum_{i=\beta}^{N} k_{abs,i}$, where N is the number of remaining carbon sites (i.e., 4 for *n*-pentanol, 5 for *n*-hexanol). Decomposition and isomerization rate constants (reaction classes 4 and 5) are obtained through the steady-state approximation at T = 1000 K, as described by Ranzi et al.,[90] from the reference kinetic parameters reported in Table 2. Interactions of radicals (B) and (A) with O_2, forming $HȮ_2$ and a C_n enol, or an aldehyde, are as described in Table 2.

Horizontal lumping is very useful to describe low-temperature-oxidation pathways by means of pseudospecies (lumped species) representative of the different types of intermediates: hydroxyalkyl peroxy radicals ($RȮ_2$), hydroperoxyl alkyl radicals ($ĊOOH$), C_n enols, C_n epoxy alcohols, ketohydroperoxides of the parent C_n alkane, hydroxyl peroxy-hydroperoxy-alkyl radicals $Ȯ_2ĊOOH$, C_n carbonyl alkyl hydroperoxides. Beside the computational advantage of this important reduction in the number of species, the introduction of one single lumped component for any intermediate radicals and compounds makes the comprehensive description of their successive reactions easier to manage and also to understand and interpret. Comprehensive kinetic mechanisms available in the literature often describe the occurring chemistry in a very detailed fashion only until where the explosion of the number of species (e.g., in ketohydroperoxides) forces the treatment of every isomer with the same kinetic rate constant, based on analogy. This is justified by the fact that not every rate constant for every specific intermediate species has been determined, theoretically or experimentally. This coexistence of the aim for a high level of detail and difficulties in managing the complexity of combustion kinetic mechanisms, and the unavailability of specific rate constants for every isomer, further supports the suitability, efficiency, convenience, and robustness of the lumped approach largely applied in previous developments of the CRECK kinetic model. The lumped kinetic parameters are then derived through an optimization process aimed at minimizing the deviation in the selectivities to final products (i.e., $ĊOOH$, $Ȯ_2ĊOOH$, epoxy

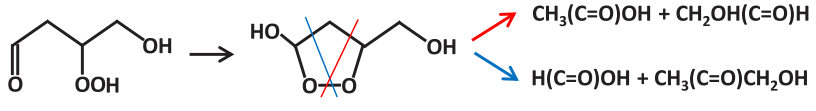

Figure 13. Example of Korcek mechanism decomposition of CHHP in *n*-butanol oxidation.

https://dx.doi.org/10.1021/acs.energyfuels.0c02251
Energy Fuels 2020, 34, 14688−14707

Table 3. Reference Kinetic Parameters for the Low-Temperature Oxidation of Alcohols[a]

Addition reactions of hydroxy alkyl radicals to O_2 ($R+O_2=RO_2$) and second addition $QOOH+O_2=OOQOOH$									
		A	**n**	**Ea**	**A**	**n**	**Ea**		
		Primary radical			*Secondary radical*				
		$1.0\ 10^{12}$	0.0	0	$2.0\ 10^{12}$	0.0	0		
Recombination/disproportionation $R'+RO_2=RO+RO$ ($R'=H$, CH_3, alcohol radicals)									
		$3.5\ 10^{12}$	0.0	-1000					
Recombination/disproportionation $R'O_2+RO_2=RO+RO$ ($R=H$, CH_3, alcohol radicals)									
R=H			*R=CH 3*			*R=alcohol radicals*			
$3.0\ 10^{10}$	0.0	-1200	$2.0\ 10^{10}$	0.0	0.0	$2.0\ 10^{10}$	0.0	0.0	
RO_2 concerted eliminations to form HO_2+aldehyde/enol									
		$3.0\ 10^{37}$	0.0	39500					
RO_2 isomerizations (RO_2=QOOH)*									
1p, c5			*1p, c6*			*1s, c5*			*1s, c6*
$1.0\ 10^{11.8}$	0.0	28500	$1.0\ 10^{11.0}$	0.0	22500	$1.0\ 10^{11.8}$	0.0	26200	$1.0\ 10^{11.0}$	0.0	22200
1s β, c5			*1s* β, c6			*1s* α, c5			*1s* α, c6		
$1.0\ 10^{11.8}$	0.0	27200	$1.0\ 10^{11.0}$	0.0	21200	$1.0\ 10^{11.8}$	0.0	24500	$1.0\ 10^{11.0}$	0.0	18500
Waddington mechanism (RO_2=OH+CH_2O+C_{n-1} aldehyde)									
		$9.0\ 10^{10.0}$	0.0	22000					
QOOH (radical in γ to OOH) decomposition to form OH+alkenes/enols+carbonyl compounds									
		$1.0\ 10^{13.2}$	0.0	22500					
QOOH (radical in β to OOH) decomposition to form HO_2+C_n Enols									
		$1.0\ 10^{14.0}$	0.0	24000					
QOOH decomposition to form OH and epoxy alcohols									
3-member cyclic structure			*4-member cyclic structure*			*5-member cyclic structure*			
$1.0\ 10^{12.0}$	0.0	18000	$1.0\ 10^{11.2}$	0.0	17000	$1.0\ 10^{10.4}$	0.0	8500	
QOOH dehydration									
		$4.0\ 10^{10.0}$	0.0	13000					
Decomposition of carbonyl hydroxyalkyl hydroperoxides (branching)									
		$1.0\ 10^{16.0}$	0.0	40000					
Decomposition of carbonyl hydroxyalkyl hydroperoxides with Korcek mechanism									
		$1.0\ 10^{2.0}$	2.13	27500					
H-abstractions on carbonyl hydroxyalkyl hydroperoxides									
		by $\dot{O}H$			*by $H\dot{O}_2$*				
		$1.0\ 10^{13.0}$	0.0	630	$5.0\ 10^{12.0}$	0.0	12460		

[a]Units are cal, cm^3, mol, s. Note: the asterisk symbol (*) denotes that the second isomerization involves a correction (−1200 cal/mol) to account for the weaker C−H bond due to −OOH substitution.

alcohols, enols, CHHP, etc.) between the original detailed mechanism and the lumped one, as previously described.[73,74,81,89−91,94]

Decomposition reactions of CHHP via O−OH bond fission are written in a lumped way and stoichiometric coefficients are assigned to the reaction products (e.g., $C_4CHHP \rightarrow OH + 0.5\dot{C}H_2CHO + 0.5CH_2OHCHO + 0.5CH_2O + 0.5CO + 0.5P\dot{C}_2H_4OH$). The stoichiometric coefficients are determined at a reference intermediate temperature ($T = 800$ K, in this case), to better reflect the temperature dependence of the specific channels in the low-temperature branching pathways, leading to the formation of different CHHP (Figure 12) and, therefore, a variable distribution of products. However, note that modifications to the relative distributions do not significantly impact the overall reactivity nor the formation of product species, because the flux reaching CHHP species is typically very limited for alcohols, particularly for the conditions under which experimental data are available. Figure 14 compares the distribution of products from CHHP decomposition from the reference kinetic parameters discussed in the previous section, and from the lumped model.

Table 4 shows lumped kinetic parameters for low-temperature reaction pathways for *n*-propanol, *n*-butanol, and *n*-pentanol. As determined by Ranzi et al.[74] for a series of *n*-alkanes, it is reasonable to directly extend the kinetic parameters of *n*-pentanol to higher-molecular-weight alcohols (e.g., *n*-hexanol, *n*-octanol). In the case of alcohol fuels, this is further justified by the decreasing importance of the alcohol specific moiety for increasing molecular weight. Concerning the first addition to O_2 ($\dot{R} + O_2 \leftrightarrow R\dot{O}_2$), for *n*-propanol and *n*-butanol, the fuel radicals are described in detail in the kinetic model. Table 4 reports the sum of the individual rate constants assigned

https://dx.doi.org/10.1021/acs.energyfuels.0c02251
Energy Fuels 2020, 34, 14688−14707

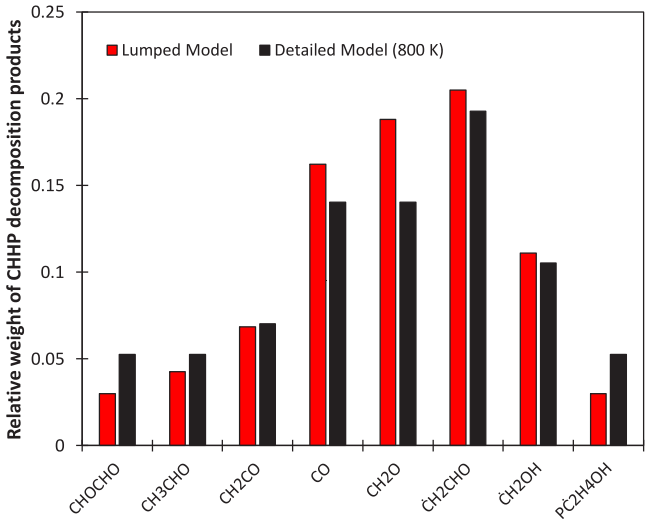

Figure 14. Relative weight of CHHP decomposition products in the lumped model and in the detailed model (T = 800 K).

according to the reference kinetic parameters discussed in Section 2.7. For *n*-pentanol and higher-molecular-weight alcohols, one single lumped radical (B) adds to O_2. However, from the increasing carbon chain length, one would expect that the rate constants for addition reactions rank in the following order: *n*-pentanol > *n*-butanol > *n*-propanol. However, according to the lumping approach adopted here,[90] the rate constant for $\dot{R} + O_2$ (k_{lump}) is derived from a weighted average, considering the relative branching to the different isomers (i.e., the fuel radicals) of H-atom abstraction reactions by ȮH and $H\dot{O}_2$ at the reference temperature of 700 K. Therefore, the rate constant is lower for *n*-pentanol, but the impact of the chain length is implicitly taken into account in the concentration of [Ṙ], which is the sum of the concentrations of the different isomers, from which a higher addition rate is obtained as $r = k_{lump}[\dot{R}_{pentanol}][O_2]$ (in units of mol/cm^3/s).

Figure 15 demonstrates the validity of the lumping approach described above by comparing the profiles of relevant species in the low-temperature oxidation pathways of *n*-pentanol obtained with the detailed kinetic model of Sarathy et al.[5] and with the lumped kinetic model presented in this work. Results are obtained from a simulation in an adiabatic constant volume batch reactor. The two models predict very similar values of the IDT (∼9.4 ms) at T = 900 K, p = 10 bar, and φ = 1.0. The minor difference in the fuel conversion profiles, justified by slightly different rate constants for the H atom abstraction reactions, is responsible for the differences in the mole fraction profiles of intermediate species at early times preceding the ignition event.

$H\dot{O}_2$ radicals are produced by the interaction of O_2 with α-radicals, forming *n*-pentanal, and they are consumed by H-atom abstraction from the fuel molecule, and by the termination reaction $H\dot{O}_2 + H\dot{O}_2 = H_2O_2 + O_2$; further decomposition of H_2O_2, producing two ȮH radicals, drives the onset of ignition. Despite similar shapes, our lumped model predicts higher yields of α-radicals (∼1 order of magnitude) and lower yields of the remaining alkyl radicals. This difference propagates throughout the low-temperature branching pathways that is primarily derived from the oxidation of the remaining alkyl radicals. Indeed, the Sarathy et al. model predicts higher yields of $R\dot{O}_2$, Q̇OOH, epoxy alcohols, and $\dot{O}_2$QOOH. Figure 16 shows a rate of production analysis at 20% fuel conversion for the same conditions of Figure 15.

The different isomers of the low-temperature branching pathways described in detail by Sarathy et al.[5] (77 species) have been grouped to resemble the lumped species (9 species). The main differences between the two kinetic models arise from the selectivity of H-atom abstraction reactions. The selectivity to α-radical $R_{(A)}$ is 35% for our model and 45% in the model of Sarathy et al. Nearly all of the formed $R_{(A)}$ is converted to *n*-pentanal in the CRECK model, while ∼5% combines with O_2, producing $R\dot{O}_2$, according to Sarathy.[5] Different rate parameters justify the higher importance of β-scission reactions in Sarathy et al.[5] (see Figure S1), while our kinetic model proposes a

Table 4. Kinetic Parameters of the Lumped Low-Temperature Reactions of *n*-C_3−C_5 Alcohols[a]

	n-Propanol			*n*-Butanol			*n*-Pentanol		
lumped reactions	A	n	E_a	A	n	E_a	A	n	E_a
$R + O_2 \leftrightarrow R\dot{O}_2$*	3.0×10^{12}	0.00	0.0	4.0×10^{12}	0.00	0.0	1.2×10^{12}	0.00	0.0
	3.0×10^{13}	*0.00*	*30000.*	*3.0×10^{13}*	*0.00*	*30000.*	*3.0×10^{13}*	*0.00*	*30000.*
$R\dot{O}_2 \leftrightarrow$ Q̇OOH	1.3×10^{6}	1.51	18449.	4.2×10^{9}	0.39	19621.	2.2×10^{3}	2.46	17204.
	3.4×10^{9}	*0.29*	*12513.*	*1.8×10^{9}*	*1.60*	*11124.*	*6.0×10^{3}*	*2.19*	*10839.*
$RO_2 \rightarrow$ ȮH + CH_2O + C_{n-2} *aldehyde (Waddington)*	1.5×10^{10}	0.00	22000.	1.5×10^{10}	0.00	22000.	1.5×10^{10}	0.00	22000.
Q̇OOH *(radical in γ to OOH)* → ȮH + *alkenes/enols + carbonyl*	1.0×10^{16}	−1.01	23327.	1.0×10^{16}	−1.01	23327.	1.2×10^{17}	−1.34	23538.
Q̇OOH *(radical in β to OOH)* → $H\dot{O}_2$ + C_n *enol*	5.1×10^{7}	1.82	23182.	5.1×10^{7}	1.82	23182.	5.9×10^{12}	0.48	27345.
Q̇OOH → ȮH + *epoxy alcohols*	1.7×10^{10}	0.37	17120.	2.8×10^{10}	0.37	17120.	2.8×10^{10}	0.37	17120.
Q̇OOH → H_2O + HĊO + C_{n-1} *aldehyde*	4.0×10^{10}	0.00	13000.	4.0×10^{10}	0.00	13000.	4.0×10^{10}	0.00	13000.
α-Q̇OOH + $O_2 \rightarrow H\dot{O}_2$ + C_n *alkane ketohydroperoxide*	7.5×10^{10}	0.30	−1069.	7.5×10^{10}	0.30	−1069.	7.5×10^{10}	0.30	−1069.
Q̇OOH + $O_2 \leftrightarrow \dot{O}_2$QOOH	2.5×10^{12}	0.00	0.0	2.5×10^{12}	0.00	0.0	2.5×10^{12}	0.00	0.0
	3.0×10^{13}	*0.00*	*30000.*	*3.0×10^{13}*	*0.00*	*30000.*	*3.0×10^{13}*	*0.00*	*30000.*
$\dot{O}_2$QOOH → ȮH + *carbonyl hydroxyalkyl hydroperoxides*	1.3×10^{6}	1.51	17249.	4.2×10^{9}	0.4	18421.	2.2×10^{3}	2.5	16004.
carbonyl hydroxyalkyl hydroperoxides → ȮH + *radicals*	$1. \times 10^{16}$	0.0	40000.	$1. \times 10^{16}$	0.0	40000.	1.0×10^{16}	0.0	40000.

[a]Notes: Units are cm^3, mol, s, cal. The asterisk symbol (*) represents a detailed fuel radicals (R) description for *n*-propanol and *n*-butanol; rate parameters reported in the table are the sum of the individual rate constants. Reverse lumped rate constants are shown in italic font.

https://dx.doi.org/10.1021/acs.energyfuels.0c02251
Energy Fuels 2020, 34, 14688−14707

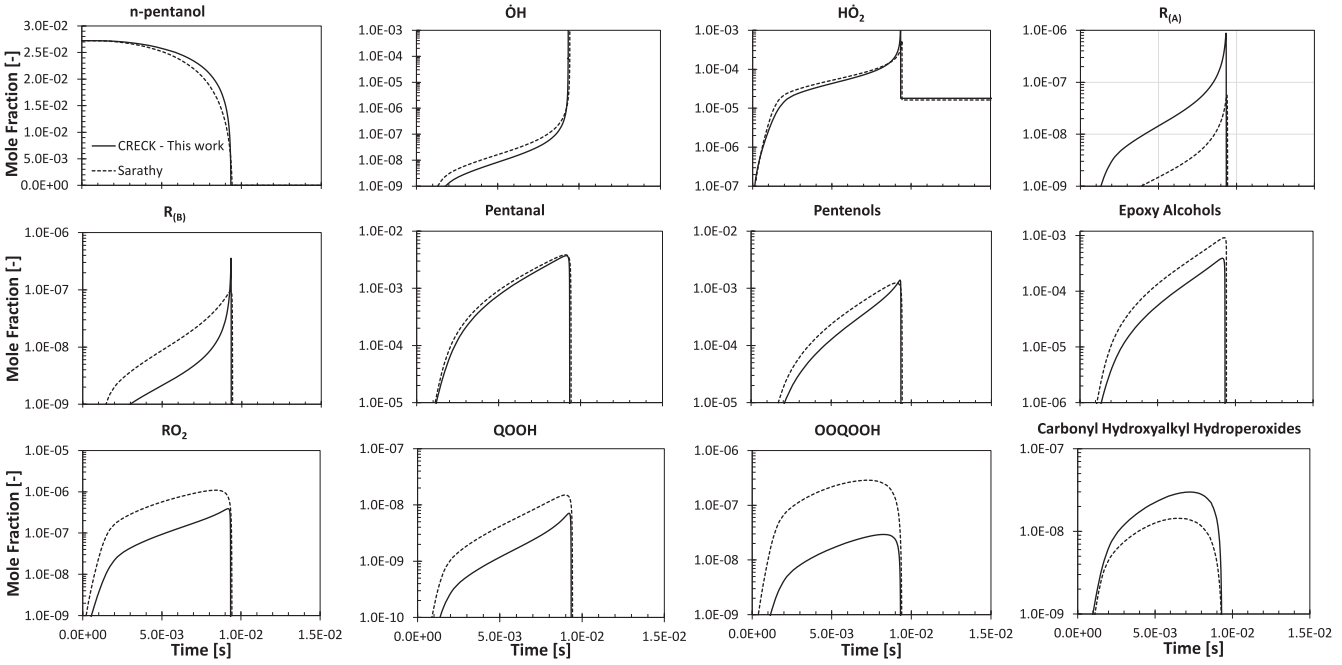

Figure 15. Simulated mole fraction profiles of relevant species in the oxidation of an *n*-pentanol/air mixture in an adiabatic constant volume batch reactor (T = 900 K, p = 10 bar, φ = 1.0). Solid lines represent the lumped model from this work, dashed lines represent the detailed model from Sarathy et al.[5]

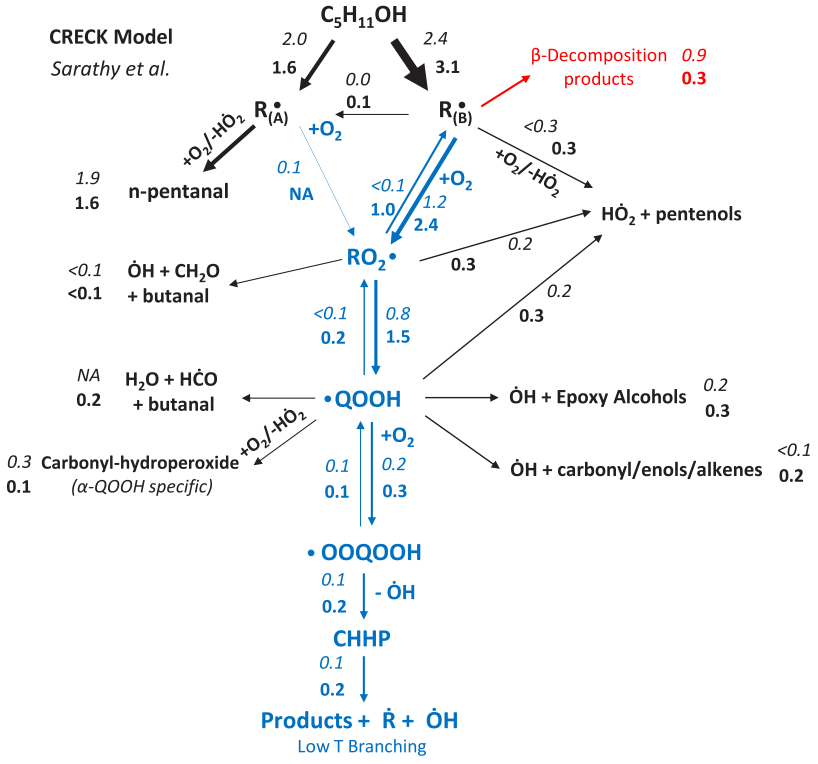

Figure 16. Flux analysis of *n*-pentanol oxidation in an adiabatic constant volume batch reactor at T = 900 K, p = 10 bar, and φ = 1.0 (fuel conversion of ~20%). Numbers are rates of production/consumption in 10^{-4} mol cm^{-3} s^{-1}. Bold font denotes data obtained using the CRECK model; italic font denotes data obtained from Sarathy et al.[5] NA indicates that the pathway was not available in the model.

preferential addition to O_2 toward the low-temperature chain-branching pathways. This effect is counterbalanced by higher backward rates for $R\dot{O}_2 = \dot{R} + O_2$ and by a higher formation of pentenol isomers and $H\dot{O}_2$ radicals. A minor difference is also observed for the isomerization reactions leading to $\dot{R}_{(A)}$. $R\dot{O}_2$ radicals mostly isomerize to $\dot{Q}OOH$ in both models, with the CRECK model predicting a higher flux of the backward reaction. Similar fluxes are observed for the decomposition of $R\dot{O}_2$ to $H\dot{O}_2$ and the pentenol isomers. The low importance of the Waddington mechanism producing ȮH, formaldehyde, and *n*-butanal is consistent between the two models. Because of the relatively high-temperature conditions, the second addition to

https://dx.doi.org/10.1021/acs.energyfuels.0c02251
Energy Fuels 2020, 34, 14688−14707

Table 5. Synopsis of Validation Targets and Model Performances[a56]

Reference	Exp. Device	Example of results
Pyrolysis Speciation, Hefei [54, 55, 83]	Flow reactor, Molecular beam mass spectrometry	*T* = 900−1400 K, *p* = 150−200 Torr, φ = ∞, 3% mol fuel/Ar. 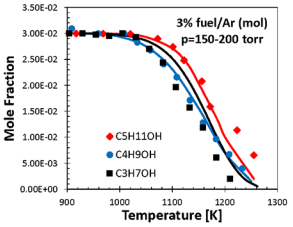
Pyrolysis Speciation, Ghent [37, 59]	Flow Reactor, gas chromatography	*T* = 640 − 810 °C, *p* = 1.7 bar, φ = ∞, 50% mol fuel/N_2. 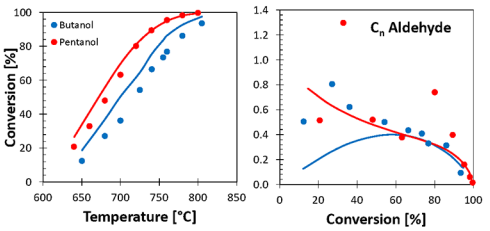
Laminar Flame Speed [54, 60, 61, 96-98]	Constant volume combustion vessel, Heat Flux Burner	*T* = 423 K, *p* = 1 atm, φ = 0.7−1.7. 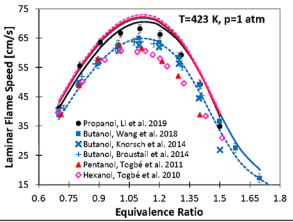
Ignition Delay Time [50, 99-103]	Shock tube	*T* = 700−1700 K, *p* = 1−30 bar, φ = 0.25−2.00. 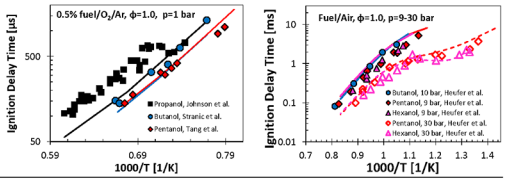
Ignition Delay Time [56, 104]	Rapid Compression Machine	*T* = 650− 950 K, *p* = 10 bar, φ = 1.0. 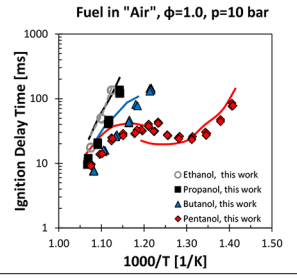
Oxidation speciation, JSR Nancy [56]	Jet Stirred Reactor, gas chromatography mass spectrometry (GC-MS)	*T* = 500−1100 K, *p* = 1.07 bar, φ = 1.0 (0.5% mol fuel/O_2/He), τ = 2.0 s. 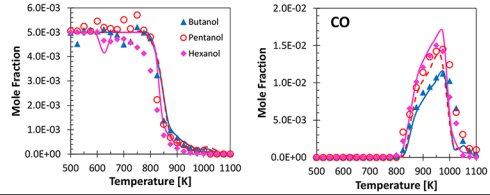
Oxidation speciation, JSR Orleans [58, 60, 61, 72]	Jet Stirred Reactor, gas chromatography mass spectrometry (GC-MS)	*T* = 550−1150 K, *p* = 10 bar, φ = 0.5 (0.1% mol fuel/O_2/N_2), τ = 0.7 s. 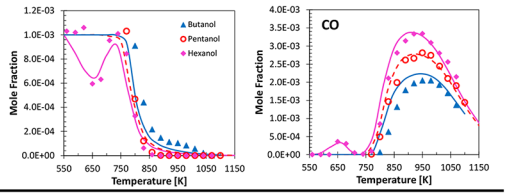

[a]Data taken from refs 37, 50, 54−56, 59−61, 83, and 96−104. For a deeper discussion, the reader is referred to Part II of this study.[56]

https://dx.doi.org/10.1021/acs.energyfuels.0c02251
Energy Fuels 2020, 34, 14688−14707

O_2 ($\dot{Q}OOH + O_2 = \dot{O}_2QOOH$) is of minor importance, compared to the $\dot{Q}OOH$ decomposition pathways (20% vs 80%). The same flux is then conserved until the branching decomposition reactions of CHHP.

From this graphical representation, it is possible to conclude the following:

(1) the CRECK model proposes a higher influence of the chemical equilibrium in the low-temperature branching pathways, thus justifying the differences in the yields of $R\dot{O}_2$, $\dot{Q}OOH$, and $\dot{O}_2QOOH$ highlighted in Figure 15; and

(2) the higher flux undergoing the low-temperature branching pathway in the CRECK model is counter-balanced by a higher importance of backward reactions and propagation pathways, such as the decompositions of $\dot{Q}OOH$ and $R\dot{O}_2$ radicals.

Globally, the similar balance between branching and propagation pathways justifies the similar reactivity. A similar analysis, for lower-temperature conditions (T = 748 K) is reported in Figure S2 in the Supporting Information, further supporting the governing role of relative contributions, in terms of global reactive fluxes between competing pathways (e.g., low-temperature branching vs propagation/termination reactions) rather than the absolute values of rate constants when the goal is to reproduce macroscopic targets such as IDTs. The satisfactory agreement of the lumped model proposed here with detailed speciation data over a wide range of conditions for the different fuels further supports the selected parameters and the reliability of the simplifications proposed here.

4. PRELIMINARY MODEL VALIDATION

Because of space limitations, in this section, we only present a synopsis of the overall performances of the model (see Table 5). A detailed description of the experimental setups of the jet-stirred reactor and of the rapid compression machine used in this study are presented in Part II of this study,[56] together with a more-detailed discussion on model validation and performances. Model simulations have been performed using the OpenSMOKE++ solvers by Cuoci et al.[95]

5. CONCLUSIONS

Considering new experimental measurements that have been performed in this work (see Part II in this study[56]), as well as the large amount of experimental data on alcohol pyrolysis and combustion available in the literature, the alcohol subset of the CRECK kinetic model developed in previous kinetics studies[51−53] has been updated and systematically extended to describe the low-temperature oxidation of *n*-butanol, *n*-pentanol, and *n*-hexanol at low temperatures. The kinetic model is developed based on the reaction class and rate rules approach, and a thorough discussion of the different classes and of the reference kinetic parameters is provided. The underlying assumption upon which the model has been developed is that it is possible to simplify the description of alcohol fuels from *n*-propanol, assuming an alkane-like moiety and an alcohol-specific moiety. Based on a recent review[5] and on previous theoretical and kinetic modeling studies, reference kinetic parameters for alcohol-specific reaction pathways have been defined also, correcting rate rules for alkane fuels by taking into account the peculiar features (e.g., BDE) induced by the presence of the hydroxyl function. The reference kinetic parameters thus defined have been systematically applied to the entire *n*-C_3−C_6 alcohol series, and the application of lumping techniques allowed us to obtain an effective and compact description. As a further proof of concept, the same approach has been further extended to *n*-octanol (see Part II in this study[56]). The model obtained generally shows good agreement over the wide range of conditions considered for the validation. The CRECK model attached to this study also describes the oxidation of other real fuel components (*n*-alkanes, *iso*-alkanes, aromatics, cycloalkanes, etc.) and the formation of pollutants (NOx, PAHs, soot), thus constituting a useful tool for fuel design.

■ ASSOCIATED CONTENT

Supporting Information

The Supporting Information is available free of charge at https://pubs.acs.org/doi/10.1021/acs.energyfuels.0c02251.

Structure and size of the kinetic models attached; nomenclature for alcohols and related molecules; comparison of radical decomposition and isomerization rate constants; rate of production analysis (PDF)
Kinetics Model 1 (TXT)
Thermodynamics Model 1 (TXT)
Kinetics Model 2 (TXT)
Thermodynamics Model 2 (TXT)
Kinetics Model 3 (TXT)
Thermodynamics Model 3 (TXT)
Transport Model 3 (TXT)
Kinetics Model 4 (TXT)
Thermodynamics Model 4 (TXT)
Transport Model 4 (TXT)
Kinetics Model 5 (TXT)
Thermodynamics Model 5 (TXT)
Transport Model 5 (TXT)
Octanol_lumped_kinetics_subset (TXT)

■ AUTHOR INFORMATION

Corresponding Author

M. Pelucchi − *CRECK Modeling Lab, Department of Chemistry Materials and Chemical Engineering, Politecnico di Milano, 20133 Milano, Italy;* orcid.org/0000-0003-3106-0236; Phone: +39 02 2399 4234; Email: matteo.pelucchi@polimi.it

Authors

S. Namysl − *Laboratoire Réactions et Génie des Procédés, CNRS, Université de Lorraine, ENSIC, Nancy Cedex, France*

E. Ranzi − *CRECK Modeling Lab, Department of Chemistry Materials and Chemical Engineering, Politecnico di Milano, 20133 Milano, Italy;* orcid.org/0000-0002-1395-6074

A. Rodriguez − *Laboratoire Réactions et Génie des Procédés, CNRS, Université de Lorraine, ENSIC, Nancy Cedex, France*

C. Rizzo − *CRECK Modeling Lab, Department of Chemistry Materials and Chemical Engineering, Politecnico di Milano, 20133 Milano, Italy*

K. P. Somers − *Combustion Chemistry Centre, National University of Ireland Galway, Galway, Ireland*

Y. Zhang − *State Key Laboratory of Multiphase Flow in Power Engineering, Xi'an Jiaotong University, Xi'an 710049, China*

https://dx.doi.org/10.1021/acs.energyfuels.0c02251
Energy Fuels 2020, 34, 14688−14707

O. Herbinet − *Laboratoire Réactions et Génie des Procédés, CNRS, Université de Lorraine, ENSIC, Nancy Cedex, France;* orcid.org/0000-0002-2155-098X

H. J. Curran − *Combustion Chemistry Centre, National University of Ireland Galway, Galway, Ireland;* orcid.org/0000-0002-5124-8562

F. Battin-Leclerc − *Laboratoire Réactions et Génie des Procédés, CNRS, Université de Lorraine, ENSIC, Nancy Cedex, France;* orcid.org/0000-0001-8265-7492

T. Faravelli − *CRECK Modeling Lab, Department of Chemistry Materials and Chemical Engineering, Politecnico di Milano, 20133 Milano, Italy*

Complete contact information is available at: https://pubs.acs.org/10.1021/acs.energyfuels.0c02251

Notes

The authors declare no competing financial interest.

■ ACKNOWLEDGMENTS

The authors at Politecnico di Milano and CNRS-Nancy acknowledge the financial support of the IMPROOF Project (No. H2020-IND-CE-2016-17/H2020-SPIRE-S016) European Union's Horizon 2020 research and innovation program (Grant Agreement No. 723706). The authors from NUI Galway acknowledge funding from Science Foundation Ireland (SFI), via Project Nos. 15/IA/3177 and 16/SP/3829.

■ REFERENCES

(1) Awad, O. I.; Mamat, R.; Ali, O. M.; Sidik, N.; Yusaf, T.; Kadirgama, K.; Kettner, M. Alcohol and ether as alternative fuels in spark ignition engine: A review. *Renewable Sustainable Energy Rev.* **2018**, *82*, 2586−2605.

(2) Kohse-Höinghaus, K.; Oßwald, P.; Cool, T. A.; Kasper, T.; Hansen, N.; Qi, F.; Westbrook, C. K.; Westmoreland, P. R. Biofuel combustion chemistry: from ethanol to biodiesel. *Angew. Chem., Int. Ed.* **2010**, *49*, 3572−3597.

(3) Kalghatgi, G. T. The outlook for fuels for internal combustion engines. *Int. J. Engine Res.* **2014**, *15*, 383−398.

(4) Morgan, N.; Smallbone, A.; Bhave, A.; Kraft, M.; Cracknell, R.; Kalghatgi, G. Mapping surrogate gasoline compositions into RON/MON space. *Combust. Flame* **2010**, *157*, 1122−1131.

(5) Sarathy, S. M.; Oßwald, P.; Hansen, N.; Kohse-Höinghaus, K. Alcohol combustion chemistry. *Prog. Energy Combust. Sci.* **2014**, *44*, 40−102.

(6) Murphy, M. J.; Taylor, J. D.; McCormick, R. L. *Compendium of experimental cetane number data*; National Renewable Energy Laboratory: Golden, CO, 2004.

(7) Kumar, B. R.; Saravanan, S. Effect of exhaust gas recirculation (EGR) on performance and emissions of a constant speed DI diesel engine fueled with pentanol/diesel blends. *Fuel* **2015**, *160*, 217−226.

(8) Cai, L.; Uygun, Y.; Togbé, C.; Pitsch, H.; Olivier, H.; Dagaut, P.; Sarathy, S. M. An experimental and modeling study of n-octanol combustion. *Proc. Combust. Inst.* **2015**, *35*, 419−427.

(9) Kumar, B. R.; Saravanan, S. Effects of iso-butanol/diesel and n-pentanol/diesel blends on performance and emissions of a DI diesel engine under premixed LTC (low temperature combustion) mode. *Fuel* **2016**, *170*, 49−59.

(10) Wei, L.; Cheung, C.; Huang, Z. Effect of n-pentanol addition on the combustion, performance and emission characteristics of a direct-injection diesel engine. *Energy* **2014**, *70*, 172−180.

(11) Babu, D.; Anand, R. Effect of biodiesel-diesel-n-pentanol and biodiesel-diesel-n-hexanol blends on diesel engine emission and combustion characteristics. *Energy* **2017**, *133*, 761−776.

(12) Zhu, L.; Xiao, Y.; Cheung, C.; Guan, C.; Huang, Z. Combustion, gaseous and particulate emission of a diesel engine fueled with n-pentanol (C5 alcohol) blended with waste cooking oil biodiesel. *Appl. Therm. Eng.* **2016**, *102*, 73−79.

(13) Chen, H.; Su, X.; He, J.; Xie, B. Investigation on combustion and emission characteristics of a common rail diesel engine fueled with diesel/n-pentanol/methanol blends. *Energy* **2019**, *167*, 297−311.

(14) Li, L.; Wang, J.; Wang, Z.; Xiao, J. Combustion and emission characteristics of diesel engine fueled with diesel/biodiesel/pentanol fuel blends. *Fuel* **2015**, *156*, 211−218.

(15) De Poures, M. V.; Sathiyagnanam, A.; Rana, D.; Kumar, B. R.; Saravanan, S. 1-Hexanol as a sustainable biofuel in DI diesel engines and its effect on combustion and emissions under the influence of injection timing and exhaust gas recirculation (EGR). *Appl. Therm. Eng.* **2017**, *113*, 1505−1513.

(16) Kumar, B. R.; Saravanan, S.; Rana, D.; Nagendran, A. A comparative analysis on combustion and emissions of some next generation higher-alcohol/diesel blends in a direct-injection diesel engine. *Energy Convers. Manage.* **2016**, *119*, 246−256.

(17) Pelucchi, M.; Bissoli, M.; Rizzo, C.; Zhang, Y.; Somers, K.; Frassoldati, A.; Curran, H.; Faravelli, T. A kinetic modelling study of alcohols operating regimes in a HCCI engine. *SAE International Journal of Engines* **2017**, *10*, 2354−2370.

(18) Curran, H. J. Developing detailed chemical kinetic mechanisms for fuel combustion. *Proc. Combust. Inst.* **2019**, *37*, 57−81.

(19) Somers, K. P.; Cracknell, R. F.; Curran, H. J. A chemical kinetic interpretation of the octane appetite of modern gasoline engines. *Proc. Combust. Inst.* **2019**, *37*, 4857−4864.

(20) Pelucchi, M.; Cavallotti, C.; Ranzi, E.; Frassoldati, A.; Faravelli, T. Relative reactivity of oxygenated fuels: alcohols, aldehydes, ketones, and methyl esters. *Energy Fuels* **2016**, *30*, 8665−8679.

(21) Pelucchi, M.; Namysl, S.; Ranzi, E.; Frassoldati, A.; Herbinet, O.; Battin-Leclerc, F.; Faravelli, T. An experimental and kinetic modelling study of n-C4C6 aldehydes oxidation in a jet-stirred reactor. *Proc. Combust. Inst.* **2019**, *37*, 389−397.

(22) Pelucchi, M.; Ranzi, E.; Frassoldati, A.; Faravelli, T. Alkyl radicals rule the low temperature oxidation of long chain aldehydes. *Proc. Combust. Inst.* **2017**, *36*, 393−401.

(23) Pelucchi, M.; Somers, K. P.; Yasunaga, K.; Burke, U.; Frassoldati, A.; Ranzi, E.; Curran, H. J.; Faravelli, T. An experimental and kinetic modeling study of the pyrolysis and oxidation of n-C3C5 aldehydes in shock tubes. *Combust. Flame* **2015**, *162*, 265−286.

(24) Veloo, P. S.; Dagaut, P.; Togbe, C.; Dayma, G.; Sarathy, S.; Westbrook, C. K.; Egolfopoulos, F. N. Jet-stirred reactor and flame studies of propanal oxidation. *Proc. Combust. Inst.* **2013**, *34*, 599−606.

(25) Veloo, P. S.; Dagaut, P.; Togbé, C.; Dayma, G.; Sarathy, S. M.; Westbrook, C. K.; Egolfopoulos, F. N. Experimental and modeling study of the oxidation of n-and iso-butanal. *Combust. Flame* **2013**, *160*, 1609−1626.

(26) Namysl, S.; Pelucchi, M.; Herbinet, O.; Frassoldati, A.; Faravelli, T.; Battin-Leclerc, F. A first evaluation of butanoic and pentanoic acid oxidation kinetics. *Chem. Eng. J.* **2019**, *373*, 973−984.

(27) Pelucchi, M.; Cavallotti, C.; Cuoci, A.; Faravelli, T.; Frassoldati, A.; Ranzi, E. Detailed kinetics of substituted phenolic species in pyrolysis bio-oils. *Reaction Chemistry & Engineering* **2019**, *4*, 490−506.

(28) Namysl, S.; Pelucchi, M.; Maffei, L. P.; Herbinet, O.; Stagni, A.; Faravelli, T.; Battin-Leclerc, F. Experimental and modeling study of benzaldehyde oxidation. *Combust. Flame* **2020**, *211*, 124−132.

(29) Maffei, L. P.; Pelucchi, M.; Faravelli, T.; Cavallotti, C. Theoretical study of sensitive reactions in phenol decomposition. *Reaction Chem. Eng.* **2020**, *5*, 452.

(30) Bertero, M.; de la Puente, G.; Sedran, U. Fuels from bio-oils: Bio-oil production from different residual sources, characterization and thermal conditioning. *Fuel* **2012**, *95*, 263−271.

(31) da Silva, G.; Bozzelli, J. W. Role of the α-hydroxyethylperoxy radical in the reactions of acetaldehyde and vinyl alcohol with HO2. *Chem. Phys. Lett.* **2009**, *483*, 25−29.

(32) da Silva, G.; Bozzelli, J. W.; Liang, L.; Farrell, J. T. Ethanol oxidation: Kinetics of the α-hydroxyethyl radical+ O2 reaction. *J. Phys. Chem. A* **2009**, *113*, 8923−8933.

(33) Aazaad, B.; Lakshmipathi, S. Reaction of Pentanol isomers with OH radical−A theoretical perspective. *Mol. Phys.* **2018**, *116*, 1153−1165.
(34) Daranlot, J.; Bergeat, A.; Caralp, F.; Caubet, P.; Costes, M.; Forst, W.; Loison, J. C.; Hickson, K. M. Gas-Phase Kinetics of Hydroxyl Radical Reactions with Alkenes: Experiment and Theory. *ChemPhysChem* **2010**, *11*, 4002−4010.
(35) Ferro-Costas, D.; Martínez-Núñez, E.; Rodríguez-Otero, J.; Cabaleiro-Lago, E.; Estévez, C. M.; Fernández, B.; Fernández-Ramos, A.; Vázquez, S. A. Influence of multiple conformations and paths on rate constants and product branching ratios. thermal decomposition of 1-propanol radicals. *J. Phys. Chem. A* **2018**, *122*, 4790−4800.
(36) Guo, X.; Zhang, R. M.; Gao, L. G.; Zhang, X.; Xu, X. Computational kinetics of the hydrogen abstraction reactions of n-propanol and iso-propanol by OH radical. *Phys. Chem. Chem. Phys.* **2019**, *21*, 24458−24468.
(37) Van de Vijver, R.; Van Geem, K. M.; Marin, G. B.; Zádor, J. Decomposition and isomerization of 1-pentanol radicals and the pyrolysis of 1-pentanol. *Combust. Flame* **2018**, *196*, 500−514.
(38) Zádor, J.; Fernandes, R. X.; Georgievskii, Y.; Meloni, G.; Taatjes, C. A.; Miller, J. A. The reaction of hydroxyethyl radicals with O2: A theoretical analysis and experimental product study. *Proc. Combust. Inst.* **2009**, *32*, 271−277.
(39) Mendes, J.; Zhou, C.-W.; Curran, H. J. Theoretical study of the rate constants for the hydrogen atom abstraction reactions of esters with• OH radicals. *J. Phys. Chem. A* **2014**, *118*, 4889−4899.
(40) Welz, O.; Klippenstein, S. J.; Harding, L. B.; Taatjes, C. A.; Zádor, J. Unconventional peroxy chemistry in alcohol oxidation: the water elimination pathway. *J. Phys. Chem. Lett.* **2013**, *4*, 350−354.
(41) Zhou, C. W.; Simmie, J. M.; Curran, H. J. Rate constants for hydrogen abstraction by HȮ2 from n-butanol. *Int. J. Chem. Kinet.* **2012**, *44*, 155−164.
(42) Katsikadakos, D.; Zhou, C.-W.; Simmie, J.; Curran, H.; Hunt, P.; Hardalupas, Y.; Taylor, A. Rate constants of hydrogen abstraction by methyl radical from n-butanol and a comparison of CanTherm, MultiWell and Variflex. *Proc. Combust. Inst.* **2013**, *34*, 483−491.
(43) Zhou, C.-W.; Simmie, J. M.; Curran, H. J. Rate constants for hydrogen-abstraction by ȮH from n-butanol. *Combust. Flame* **2011**, *158*, 726−731.
(44) McGillen, M. R.; Baasandorj, M.; Burkholder, J. B. Gas-phase rate coefficients for the OH+ n-, i-, s-, and t-butanol reactions measured between 220 and 380 K: Non-arrhenius behavior and site-specific reactivity. *J. Phys. Chem. A* **2013**, *117*, 4636−4656.
(45) Pang, G. A.; Hanson, R. K.; Golden, D. M.; Bowman, C. T. Rate constant measurements for the overall reaction of OH+ 1-butanol→ products from 900 to 1200 K. *J. Phys. Chem. A* **2012**, *116*, 2475−2483.
(46) Rajakumar, B.; McCabe, D. C.; Talukdar, R. K.; Ravishankara, A. Rate coefficients for the reactions of OH with n-propanol and iso-propanol between 237 and 376 K. *Int. J. Chem. Kinet.* **2010**, *42*, 10−24.
(47) Sivaramakrishnan, R.; Su, M.-C.; Michael, J.; Klippenstein, S.; Harding, L.; Ruscic, B. Rate constants for the thermal decomposition of ethanol and its bimolecular reactions with OH and D: reflected shock tube and theoretical studies. *J. Phys. Chem. A* **2010**, *114*, 9425−9439.
(48) Yujing, M.; Mellouki, A. Temperature dependence for the rate constants of the reaction of OH radicals with selected alcohols. *Chem. Phys. Lett.* **2001**, *333*, 63−68.
(49) Vasu, S. S.; Davidson, D. F.; Hanson, R. K.; Golden, D. M. Measurements of the reaction of OH with n-butanol at high-temperatures. *Chem. Phys. Lett.* **2010**, *497*, 26−29.
(50) Heufer, K. A.; Sarathy, S. M.; Curran, H. J.; Davis, A. C.; Westbrook, C. K.; Pitz, W. J. Detailed kinetic modeling study of n-pentanol oxidation. *Energy Fuels* **2012**, *26*, 6678−6685.
(51) Frassoldati, A.; Cuoci, A.; Faravelli, T.; Niemann, U.; Ranzi, E.; Seiser, R.; Seshadri, K. An experimental and kinetic modeling study of n-propanol and iso-propanol combustion. *Combust. Flame* **2010**, *157*, 2−16.
(52) Grana, R.; Frassoldati, A.; Faravelli, T.; Niemann, U.; Ranzi, E.; Seiser, R.; Cattolica, R.; Seshadri, K. An experimental and kinetic modeling study of combustion of isomers of butanol. *Combust. Flame* **2010**, *157*, 2137−2154.
(53) Nativel, D.; Pelucchi, M.; Frassoldati, A.; Comandini, A.; Cuoci, A.; Ranzi, E.; Chaumeix, N.; Faravelli, T. Laminar flame speeds of pentanol isomers: An experimental and modeling study. *Combust. Flame* **2016**, *166*, 1−18.
(54) Li, W.; Zhang, Y.; Mei, B.; Li, Y.; Cao, C.; Zou, J.; Yang, J.; Cheng, Z. Experimental and kinetic modeling study of n-propanol and i-propanol combustion: Flow reactor pyrolysis and laminar flame propagation. *Combust. Flame* **2019**, *207*, 171−185.
(55) Wang, G.; Yuan, W.; Li, Y.; Zhao, L.; Qi, F. Experimental and kinetic modeling study of n-pentanol pyrolysis and combustion. *Combust. Flame* **2015**, *162*, 3277−3287.
(56) Pelucchi, M.; Namysl, S.; Ranzi, E.; Rodriguez, A.; Rizzo, C.; Somers, K.; Zhang, Y.; Herbinet, O.; Curran, H.; Battin-Leclerc, F.; Faravelli, T. Combustion of n-C_3−C_6 Linear Alcohols: An Experimental and Kinetic Modeling Study. Part II: Speciation Measurement in a Jet Stirred Reactor, Ignition Delay Time Measurement in a Rapid Compression Machine, Model Validation and Kinetic Analysis. Submitted to *Energy Fuels* **2020**.
(57) Black, G.; Curran, H.; Pichon, S.; Simmie, J.; Zhukov, V. Bio-butanol: Combustion properties and detailed chemical kinetic model. *Combust. Flame* **2010**, *157*, 363−373.
(58) Dagaut, P.; Sarathy, S.; Thomson, M. A chemical kinetic study of n-butanol oxidation at elevated pressure in a jet stirred reactor. *Proc. Combust. Inst.* **2009**, *32*, 229−237.
(59) Harper, M. R.; Van Geem, K. M.; Pyl, S. P.; Marin, G. B.; Green, W. H. Comprehensive reaction mechanism for n-butanol pyrolysis and combustion. *Combust. Flame* **2011**, *158*, 16−41.
(60) Togbé, C.; Halter, F.; Foucher, F.; Mounaïm-Rousselle, C.; Dagaut, P. Experimental and detailed kinetic modeling study of 1-pentanol oxidation in a JSR and combustion in a bomb. *Proc. Combust. Inst.* **2011**, *33*, 367−374.
(61) Togbe, C.; Dagaut, P.; Mzé-Ahmed, A.; Diévart, P.; Halter, F.; Foucher, F. Experimental and detailed kinetic modeling study of 1-hexanol oxidation in a pressurized jet-stirred reactor and a combustion bomb. *Energy Fuels* **2010**, *24*, 5859−5875.
(62) Faravelli, T.; Frassoldati, A.; Cuoci, A.; Mehl, M.; Pelucchi, M.; Stagni, A.; Ranzi, E. *CRECK Modeling Lab*. Available via the Internet at: http://creckmodeling.chem.polimi.it/menu-kinetics/, 2020.
(63) Pejpichestakul, W.; Ranzi, E.; Pelucchi, M.; Frassoldati, A.; Cuoci, A.; Parente, A.; Faravelli, T. Examination of a soot model in premixed laminar flames at fuel-rich conditions. *Proc. Combust. Inst.* **2019**, *37*, 1013−1021.
(64) Song, Y.; Marrodán, L.; Vin, N.; Herbinet, O.; Assaf, E.; Fittschen, C.; Stagni, A.; Faravelli, T.; Alzueta, M.; Battin-Leclerc, F. The sensitizing effects of NO2 and NO on methane low temperature oxidation in a jet stirred reactor. *Proc. Combust. Inst.* **2019**, *37*, 667−675.
(65) Metcalfe, W. K.; Burke, S. M.; Ahmed, S. S.; Curran, H. J. A hierarchical and comparative kinetic modeling study of C1− C2 hydrocarbon and oxygenated fuels. *Int. J. Chem. Kinet.* **2013**, *45*, 638−675.
(66) Kéromnès, A.; Metcalfe, W. K.; Heufer, K. A.; Donohoe, N.; Das, A. K.; Sung, C.-J.; Herzler, J.; Naumann, C.; Griebel, P.; Mathieu, O.; et al. An experimental and detailed chemical kinetic modeling study of hydrogen and syngas mixture oxidation at elevated pressures. *Combust. Flame* **2013**, *160*, 995−1011.
(67) Burke, S. M.; Metcalfe, W.; Herbinet, O.; Battin-Leclerc, F.; Haas, F. M.; Santner, J.; Dryer, F. L.; Curran, H. J. An experimental and modeling study of propene oxidation. Part 1: Speciation measurements in jet-stirred and flow reactors. *Combust. Flame* **2014**, *161*, 2765−2784.
(68) Bagheri, G.; Ranzi, E.; Pelucchi, M.; Parente, A.; Frassoldati, A.; Faravelli, T. Comprehensive kinetic study of combustion technologies for low environmental impact: MILD and OXY-fuel combustion of methane. *Combust. Flame* **2020**, *212*, 142−155.
(69) Ruscic, B. Uncertainty quantification in thermochemistry, benchmarking electronic structure computations, and Active Thermochemical Tables. *Int. J. Quantum Chem.* **2014**, *114*, 1097−1101.

https://dx.doi.org/10.1021/acs.energyfuels.0c02251
Energy Fuels 2020, 34, 14688−14707

(70) Ruscic, B.; Pinzon, R. E.; Von Laszewski, G.; Kodeboyina, D.; Burcat, A.; Leahy, D.; Montoy, D.; Wagner, A. F. *Active Thermochemical Tables: Thermochemistry for the 21st Century*; Journal of Physics: Conference Series, No. *16*; IOP Publishing, 2005; p 561.
(71) Benson, S. W.; Buss, J. H. Additivity rules for the estimation of molecular properties. Thermodynamic properties. *J. Chem. Phys.* **1958**, *29*, 546−572.
(72) Sarathy, S. M.; Thomson, M. J.; Togbé, C.; Dagaut, P.; Halter, F.; Mounaim-Rousselle, C. An experimental and kinetic modeling study of n-butanol combustion. *Combust. Flame* **2009**, *156*, 852−864.
(73) Ranzi, E.; Cavallotti, C.; Cuoci, A.; Frassoldati, A.; Pelucchi, M.; Faravelli, T. New reaction classes in the kinetic modeling of low temperature oxidation of n-alkanes. *Combust. Flame* **2015**, *162*, 1679−1691.
(74) Ranzi, E.; Frassoldati, A.; Granata, S.; Faravelli, T. Wide-range kinetic modeling study of the pyrolysis, partial oxidation, and combustion of heavy n-alkanes. *Ind. Eng. Chem. Res.* **2005**, *44*, 5170−5183.
(75) Man, X.; Tang, C.; Zhang, J.; Zhang, Y.; Pan, L.; Huang, Z.; Law, C. K. An experimental and kinetic modeling study of n-propanol and i-propanol ignition at high temperatures. *Combust. Flame* **2014**, *161*, 644−656.
(76) Oyeyemi, V. B.; Keith, J. A.; Carter, E. A. Trends in bond dissociation energies of alcohols and aldehydes computed with multireference averaged coupled-pair functional theory. *J. Phys. Chem. A* **2014**, *118*, 3039−3050.
(77) Oyeyemi, V. B.; Krisiloff, D. B.; Keith, J. A.; Libisch, F.; Pavone, M.; Carter, E. A. Size-extensivity-corrected multireference configuration interaction schemes to accurately predict bond dissociation energies of oxygenated hydrocarbons. *J. Chem. Phys.* **2014**, *140*, No. 044317.
(78) Zhao, L.; Ye, L.; Zhang, F.; Zhang, L. Thermal decomposition of 1-pentanol and its isomers: A theoretical study. *J. Phys. Chem. A* **2012**, *116*, 9238−9244.
(79) Ranzi, E.; Gaffuri, P.; Faravelli, T.; Dagaut, P. A wide-range modeling study of n-heptane oxidation. *Combust. Flame* **1995**, *103*, 91−106.
(80) Curran, H. J.; Gaffuri, P.; Pitz, W. J.; Westbrook, C. K. A comprehensive modeling study of n-heptane oxidation. *Combust. Flame* **1998**, *114*, 149−177.
(81) Ranzi, E.; Dente, M.; Pierucci, S.; Biardi, G. Initial product distributions from pyrolysis of normal and branched paraffins. *Ind. Eng. Chem. Fundam.* **1983**, *22*, 132−139.
(82) Rosado-Reyes, C. M.; Tsang, W. Shock tube study on the thermal decomposition of n-butanol. *J. Phys. Chem. A* **2012**, *116*, 9825−9831.
(83) Cai, J.; Zhang, L.; Zhang, F.; Wang, Z.; Cheng, Z.; Yuan, W.; Qi, F. Experimental and kinetic modeling study of n-butanol pyrolysis and combustion. *Energy Fuels* **2012**, *26*, 5550−5568.
(84) Cai, J.; Yuan, W.; Ye, L.; Cheng, Z.; Wang, Y.; Zhang, L.; Zhang, F.; Li, Y.; Qi, F. Experimental and kinetic modeling study of 2-butanol pyrolysis and combustion. *Combust. Flame* **2013**, *160*, 1939−1957.
(85) Ranzi, E.; Sogaro, A.; Gaffuri, P.; Pennati, G.; Faravelli, T. A wide range modeling study of methane oxidation. *Combust. Sci. Technol.* **1994**, *96*, 279−325.
(86) Ranzi, E.; Dente, M.; Faravelli, T.; Pennati, G. Prediction of kinetic parameters for hydrogen abstraction reactions. *Combust. Sci. Technol.* **1993**, *95*, 1−50.
(87) Oganesyan, K.; Nalbandyan, A. Determination of the rate constant for the reaction of atomic hydrogen with propyl and butyl alcohols. *Izv Akad Nauk Arm SSR Khim Nauki*, **1965**.
(88) Zhang, P.; Klippenstein, S. J.; Law, C. K. Ab initio kinetics for the decomposition of hydroxybutyl and butoxy radicals of n-butanol. *J. Phys. Chem. A* **2013**, *117*, 1890−1906.
(89) Dente, M.; Bozzano, G.; Faravelli, T.; Marongiu, A.; Pierucci, S.; Ranzi, E. Kinetic modelling of pyrolysis processes in gas and condensed phase. *Adv. Chem. Eng.* **2007**, *32*, 51−166.
(90) Ranzi, E.; Dente, M.; Goldaniga, A.; Bozzano, G.; Faravelli, T. Lumping procedures in detailed kinetic modeling of gasification, pyrolysis, partial oxidation and combustion of hydrocarbon mixtures. *Prog. Energy Combust. Sci.* **2001**, *27*, 99−139.
(91) Ranzi, E.; Frassoldati, A.; Stagni, A.; Pelucchi, M.; Cuoci, A.; Faravelli, T. Reduced kinetic schemes of complex reaction systems: fossil and biomass-derived transportation fuels. *Int. J. Chem. Kinet.* **2014**, *46*, 512−542.
(92) Ray, D.; Waddington, D. Gas phase oxidation of alkenes—Part II. The oxidation of 2-methylbutene-2 and 2, 3-dimethylbutene-2. *Combust. Flame* **1973**, *20*, 327−334.
(93) Li, Y.; Zhao, Q.; Zhang, Y.; Huang, Z.; Sarathy, S. M. A Systematic Theoretical Kinetics Analysis for the Waddington Mechanism in the Low-Temperature Oxidation of Butene and Butanol Isomers. *J. Phys. Chem. A* **2020**, *124*, 5646−5656.
(94) Ranzi, E.; Faravelli, T.; Gaffuri, P.; Sogaro, A. Low-temperature combustion: automatic generation of primary oxidation reactions and lumping procedures. *Combust. Flame* **1995**, *102*, 179−192.
(95) Cuoci, A.; Frassoldati, A.; Faravelli, T.; Ranzi, E. OpenSMOKE++: An object-oriented framework for the numerical modeling of reactive systems with detailed kinetic mechanisms. *Comput. Phys. Commun.* **2015**, *192*, 237−264.
(96) Wang, G.; Li, Y.; Yuan, W.; Wang, Y.; Zhou, Z.; Liu, Y.; Cai, J. Investigation on laminar flame propagation of n-butanol/air and n-butanol/O2/He mixtures at pressures up to 20 atm. *Combust. Flame* **2018**, *191*, 368−380.
(97) Knorsch, T.; Zackel, A.; Mamaikin, D.; Zigan, L.; Wensing, M. Comparison of different gasoline alternative fuels in terms of laminar burning velocity at increased gas temperatures and exhaust gas recirculation rates. *Energy Fuels* **2014**, *28*, 1446−1452.
(98) Broustail, G.; Seers, P.; Halter, F.; Moréac, G.; Mounaïm-Rousselle, C. Experimental determination of laminar burning velocity for butanol and ethanol iso-octane blends. *Fuel* **2011**, *90*, 1−6.
(99) Johnson, M. V.; Goldsborough, S. S.; Serinyel, Z.; O'Toole, P.; Larkin, E.; O'Malley, G.; Curran, H. J. A shock tube study of n-and iso-propanol ignition. *Energy Fuels* **2009**, *23*, 5886−5898.
(100) Stranic, I.; Chase, D. P.; Harmon, J. T.; Yang, S.; Davidson, D. F.; Hanson, R. K. Shock tube measurements of ignition delay times for the butanol isomers. *Combust. Flame* **2012**, *159*, 516−527.
(101) Tang, C.; Wei, L.; Man, X.; Zhang, J.; Huang, Z.; Law, C. K. High temperature ignition delay times of C5 primary alcohols. *Combust. Flame* **2013**, *160*, 520−529.
(102) Heufer, K.; Bugler, J.; Curran, H. A comparison of longer alkane and alcohol ignition including new experimental results for n-pentanol and n-hexanol. *Proc. Combust. Inst.* **2013**, *34*, 511−518.
(103) Heufer, K.; Fernandes, R.; Olivier, H.; Beeckmann, J.; Röhl, O.; Peters, N. Shock tube investigations of ignition delays of n-butanol at elevated pressures between 770 and 1250 K. *Proc. Combust. Inst.* **2011**, *33*, 359−366.
(104) Weber, B. W.; Kumar, K.; Zhang, Y.; Sung, C.-J. Autoignition of n-butanol at elevated pressure and low-to-intermediate temperature. *Combust. Flame* **2011**, *158*, 809−819.

https://dx.doi.org/10.1021/acs.energyfuels.0c02251
Energy Fuels 2020, 34, 14688−14707